

Department of Precision and Microsystems Engineering

Design and tuning of a bi-stable compliant mechanism

S.Ö. Rietmeijer

Report no : 2022.013
Coach : T.W.A. Blad
Professor : P.G. Steeneken
Specialisation : MSD
Type of report : MSc Thesis
Date : 20 May 2022

DESIGN AND TUNING OF A BI-STABLE COMPLIANT MECHANISM

FOR USE IN ENERGY HARVESTING USING FREQUENCY UP
CONVERSION

M.Sc. Thesis

In partial fulfilment of the requirements for the degree of
Master of Science in Mechanical Engineering.
Department of Precision and Microsystems Engineering.
Delft University of Technology, Delft, The Netherlands.

by

Stijn RIETMEIJER

born in Amsterdam, The Netherlands

report nr 2022.013
Daily supervisor Dr. Ir. T.W.A. Blad
Senior supervisor Prof. Dr. P.G. Steeneken
Type of report MSc Thesis
Date 20 May 2022



Copyright © 2022 by S.Ö. Rietmeijer

An electronic version of this dissertation is available at
<http://repository.tudelft.nl/>.

CONTENTS

Summary	7
1 Introduction	1
1.1 Relevance and application	2
1.2 Vibrational energy harvesting	2
1.3 Frequency up converter	3
1.3.1 Bi-stable system	3
1.4 Ortho Planar Springs	3
1.5 Research focus	3
1.6 Thesis outline	4
2 Literature Research of Ortho Planar Springs for energy harvesting purposes	5
2.1 Introduction	6
2.2 Methods	7
2.2.1 CAD design	7
2.2.2 COMSOL analysis	7
2.2.3 DOF analysis	8
2.3 Classification	8
2.4 Results	9
2.5 Discussion	11
2.5.1 Stiffness analysis	11
2.5.2 Eigenmodes	11
2.5.3 DOF analysis	12
2.5.4 Strain	12
2.6 Conclusion	12
3 Design of a bi-stable impact based frequency up converter	15
3.1 Schematic model design	16
3.2 Bi-stable Impact-based Snap-through frequency-Up converter	17
3.2.1 Low Frequency Oscillator	17
3.2.2 High frequency Oscillator	18
3.3 Piezo	19
3.3.1 Bi-morph piezo	19
3.3.2 Piezo Buzzer	19
3.4 Fabricated design	20
4 Ortho Planar Spring inspired design and tuning	21
4.1 Design goal	22
4.2 Design concepts	22
4.2.1 Designs for analysis	25

4.3	Anslys model set-up	25
4.4	Design simulation.	26
4.4.1	Horizontal design	26
4.4.2	Vertical design	27
4.5	Parameter study.	28
4.5.1	Horizontal single.	28
4.5.2	Straight single	29
4.5.3	Results	29
4.6	Comparison.	30
4.7	Conclusion	31
5	Experimental verifications	33
5.1	Bi-Morph piezo	34
5.1.1	Eigenfrequency measurement	34
5.2	Laser-cut piezo buzzer	34
5.2.1	Eigenfrequency measurement	34
5.2.2	Stiffness estimate	35
5.2.3	Damping estimate	37
5.3	Verification ANSYS model.	38
5.4	Acceleration sweep	39
5.5	Dynamic Model.	40
5.5.1	Single mass spring damper system.	41
5.5.2	Dynamic model simulation	41
5.5.3	Model verification	41
5.6	Conclusions.	43
6	Conclusion	45
6.1	Overview of research activities	46
6.2	Successes	46
6.2.1	BISup design.	47
6.2.2	ANSYS Model	47
6.3	Unsuccessful efforts.	47
6.3.1	Bi-Morph piezo	47
6.3.2	Double Mass-Spring-Damper model.	47
6.4	Recommendations	47
6.5	Conclusion	48
A	Appendix: Vertical design simulation	49
A.1	Vertical design	49
B	Appendix: Snap through voltage measurement	51
B.1	Snap-through experiment Bi-morph piezo	51
B.2	Snap-through experiment Piezo Buzzer.	52
C	Appendix: Preload distance	55
C.1	Curved frames	55

Bibliography

References 57

SUMMARY

Nowadays sustainability is an important topic for research. Sustainable energy is being researched and harvested using windmills and solar panels. Another form of sustainable energy is kinetic-energy. This energy could be harvested from human motion or environmental vibrations. This field is called vibration energy harvesting. Vibration energy harvesting is a growing field of research looking into the possibilities of harvesting energy from vibrations. A common problem in energy harvesting is the available vibrations have a low frequency but the transducer requires a high frequency movement for the best performance. For this a frequency up converter is used, which can convert a low frequency vibration to a higher frequency vibration.

Ortho planar springs are springs fabricated in one plane, with their main direction of movement orthogonal to this plane. Ortho planar springs are widely used within MEMS-valves, but they can also be used in energy harvesting designs. A literature study is performed to gain insight in the ortho planar spring designs used in literature. An advantage for using ortho planar springs is the ease of fabrication. The springs can be made monolithic and can be easily laser cut in any desired configuration

In this work a bi-stable impact-driven snap-through based frequency up converter design was made, named the BISup. This design consists of a flat flexure clamped between two curved frames, forcing a displacement to one the endpoints and making this part bi-stable. A frequency up converter is a mechanism that can increase a vibrations frequency, allowing a transducer to easily harvest energy. A frequency up converter consists of 2 oscillators, a low frequency oscillator and a high frequency oscillator. The bi-stable flat flexure will function as the low frequency oscillator (LFO). The high frequency oscillator (HFO) is a piezo beam fixed onto the bi-stable flat flexure. This beam will start resonating in its eigenfrequency when snap-through occurs. When a vibration occurs the bi-stable flat flexure will snap to its other stable position and create an impact like vibration. The piezo starts a decaying resonance vibration and energy can be harvested.

The bi-stable flat flexure is further analysed. The goal for this part is to lower the snap-through force, to be able to operate at lower accelerations. Different designs are made, and three designs are further analysed. These designs are modelled using ANSYS and verified using a force deflection measurement. The three designs are measured and compared. The horizontal design could greatly reduce the snap-through force, compared to the more traditional straight design. However, a drawback to this horizontal design is the lowered stiffness in a stable point.

A dynamic model is made to gain insight in the dynamic behaviour of the system. This model is based on a double mass-spring-damper system. A single mass-spring-damper model is made to predict the behaviour of the flat flexure. This dynamic model is experimentally verified.

1

INTRODUCTION

1 1.1. RELEVANCE AND APPLICATION

In your daily life electrical devices are used all around you. These devices need electrical power to work. Nowadays, renewable energy is desired to be used over other forms of energy extraction. Energy harvesting is a process which generates energy from an ambient power source. Solar and wind energy are more known examples of power sources which can be harvested with solar panels and wind turbines. Other power sources such as hydro dynamic, electro magnetic or kinetic energy can also be used to harvest energy [1].

Most electrical devices make use of a battery to store energy. The batteries either get charged or replaced when they are empty. For most devices this is not a problem. However, for some devices in hard to reach places charging or replacing a battery is not always feasible. An example can be a medical devices such as a pacemaker. The battery life of a pacemaker is expected to be anywhere between 7-15 years, for most people this means they need a replacement battery [2]. Replacing a pacemaker requires surgery which can be invasive and dangerous. Not only that, but the surgeries can also be very costly. Another example are a low power sensors, used on a train track or on a bridge, to monitor the conditions of these structures. Replacing the batteries underneath a bridge can be dangerous and hard to reach. Replacing the batteries on long train tracks can be a lot of manual labour. An energy harvesting device can be used to either prolong or even replace a battery of such devices. This would require less manual labour and thus less costs.

1.2. VIBRATIONAL ENERGY HARVESTING

Earlier kinetic power was mentioned as a potential source for energy harvesting. Vibrations is an example of such a source. Vibrations are widely available and thus nice to use for energy harvesting [3]. For the pacemaker example an environmental vibration can be the vibration generated by walking around or up some stairs. Riemer et al. [4] showed high amounts of power can be measured on the body when moving around. To harvest power from an environmental vibration a transducer is needed. A transducer can convert power from a certain domain to another, in this case kinetic vibrations to electrical power. This power can be stored or used to power the device. A commonly used transducer used in vibrational energy harvesting is piezoelectric material. Piezoelectric material is a ceramic material with an interesting property. Applying a strain, such as bending, to the piezo material results in a voltage difference. This voltage difference inside the material can be converted to electrical power. Piezo material is often used because of its ease of use and its relative high power density [5]. To generate maximum power, a piezo needs to be vibrating in its resonance frequency. However, environmental vibrations won't always be vibrating on the desired frequency. Green et al. [6] shows that energy harvesters based on environmental vibrations should be able to function at low frequencies (<10Hz). Another obstacle is the available vibrations usually have a amplitude larger then the device used.

1.3. FREQUENCY UP CONVERTER

The resonance frequency of piezo material can be higher compared to the vibration available. To overcome this problem a mechanism can be made to convert the frequency of this vibration closer to the resonance frequency of the piezo material. A mechanism to convert a lower frequency vibration to a higher frequency is called a frequency up converter. In literature multiple kinds of frequency up converters are described. Another great advantage to frequency up converter designs is being able to prolong the duration of a vibration. Most of these converters consist of three things; a low frequency oscillator, a high frequency oscillator, and a coupling. This coupling couples the motion from the low frequency oscillator to the motion of the high frequency oscillator. Blad et al. [7] classifies on the basis of plucking or impact. These operating principles are important to classify and judge different designs. Pozzi et al. [8] proposes a vibrational energy harvester based on plucking.

1.3.1. BI-STABLE SYSTEM

A bi-stable system can be used within a frequency up converter as low frequency oscillator. The bi-stable system can be switched from its stable point by the environmental vibration. This switching behaviour can create an impact like vibration, this impact can be used to vibrate the high frequency oscillator. Jung [9] proposes an energy harvesting device based on impact frequency up converting. This design uses a bistable system to create this impact. This device makes use of the forces applied when snap through occurs.

1.4. ORTHO PLANAR SPRINGS

Ortho Planar Springs (OPS) are springs fabricated in a plane, with its principal direction of motion orthogonal to this plane. An advantage to using these springs is ease of fabrication, the springs are flat and monolithic, which allows the springs to be easily laser-cut. Parise et al. [10] proposed to use these springs for a pneumatic controller. The ease of fabrication also allows the springs to be scaled down to even the MEMS scale. On MEMS scale ortho planar springs are widely used to, for example, operate small valves [11–15]. These springs allow easy design of the stiffness in limited design space. Dhote et al. [16] proposes to use a OPS in an energy harvester design. This design uses piezoelectric material as transducer for this system.

1.5. RESEARCH FOCUS

This thesis describes the design and tuning of an energy harvester. The energy harvester design is a frequency up converter consisting of an bi-stable flat flexure, which functions as a low frequency oscillator, and a piezo beam with tip mass that will function as high frequency oscillator. In this design an important factor of the behaviour will be the switching force of the bi-stable unit. This force limits at what acceleration the system will switch.

This thesis proposes the use of ortho planar spring design within a bi-stable unit, with as goal to lower the switching force resulting in a better performing design. Finally

a dynamic model is proposed on the basis of a double mass-spring-damper system to represent the energy harvester design and to be able to evaluate it.

1.6. THESIS OUTLINE

In the second chapter a literature research is presented. This research focusses on the use of ortho planar spring designs. A classification is made based on the found designs and each ortho planar spring design is modelled to simulate its behaviour.

The third chapter presents the design of an bi-stable impact-driven snap-through frequency up converter (BISup). It discusses the frequency up converter parts separately. The choice for piezo transducer is discussed.

The fourth chapter discusses the different ortho planar spring designs used for the bi-stable unit. These designs are classified on appearance, similar to the literature. A design goal is made and certain designs are simulated using ANSYS.

The fifth chapter discusses all the experimental tests done. It explains how the piezo transducer was chosen. The full design is modelled as a single mass-spring-damper system, then simulated and verified using a measurement.

Finally the sixth chapter gives a conclusion to this thesis. The process for this thesis is shown. The successful and the unsuccessful attempts are discussed and shown. Recommendations for further research is made.

2

LITERATURE RESEARCH OF ORTHO PLANAR SPRINGS FOR ENERGY HARVESTING PURPOSES

This chapter contains a literature research of Ortho Planar Springs for energy harvesting purposes.

2.1. INTRODUCTION

The use of small sensors and other lower power electronics is increasing a lot. Powering these device could be improved by the use of Vibrational Energy Harvesting (VEH). VEH mechanisms are able to convert kinetic energy to electric energy. Research in this field has been growing in the last two decades. A well known transducer method to generate power from VEH is the magnetic type. VEH which make use of this transducers have been proposed by [17], where the design of a bi-stable VEH is proposed. Soliman et al. [18] proposes another magnetic VEH making use of a micro-power generator. A disadvantage about a magnetic transducer is on the small scale, where magnets are hard to use.

Another well known transducer method makes use of piezo based energy harvesting. Multiple comprehensive reviews of the state-of-the-art are done by [19, 20]. In Qian et al. [21] a piezoelectric VEH from human walking is proposed and experimentally tested. In [22] a bi-stable piezo electric VEH is proposed and measured.

Ortho Planar Springs (OPS) are springs that can be fabricated in one plane, but have a motion primarily orthogonal to this fabrication plane [10]. A great advantage to OPS is the ease of fabrication compared to more regular mechanisms. An OPS is usually monolithically fabricated and can be laser cut. For a long time OPS have been used in MEMS designs of micro-valves. In [11–15] multiple micro valves are proposed and tested. Other studies show the potential to use OPS in other manners like a force sensor for robot force control [23]. In [24] Qiu et al. proposes a continuum manipulator based on serial integration of OPS. In [25] a electrostatic MEMS actuator is proposed. More OPS designs for various uses are proposed in [26–29].

More complex OPS structures are commonly known as Lamina Emergent Mechanisms (LEMs), these can be defined as a kind of OPS [30, 31]. These mechanism mostly make use of torsional hinges to fold into their folded state [32] and usually have multiple stable configurations. These mechanism are left out of this review because these torsional hinges are not that great for piezo energy harvesting.

However, although OPSs are already widely used in multiple designs, more research is needed for designing OPSs for piezoelectric VEH purposes. Therefore it should be interesting to research OPS for implementation in piezoelectric VEH.

More recent studies show the potential of OPS for VEH purposes. A study by Tao et al. [33] desgins and implements an electrostatic VEH. In [16] a VEH is proposed for wideband harvesting purposes. In [34] a piezo VEH is proposed with a circular layout. The research objective of this work is to present an overview of the used OPS in literature. The goal is to gain insight in the design of OPS for VEH purposes. For this an overview of 20 OPS is made and 5 classes are proposed.

In Section 2.2 the method of classification and analysis is explained. The classification made is shown in section 2.3. In Section 2.4 the results are shown. These are discussed in Section 2.5. Finally, conclusions are given in Section 2.6.

2.2. METHODS

A literature study is performed to generate a list of 20 OPS used in scientific papers. Each of these OPS are remade in CAD and are made with the same outer dimensions for consistency. A initial classification has been made to classify the springs on topology. A COMSOL analysis is performed on each OPS. In figure 2.1 an OPS is shown with some definitions used further.

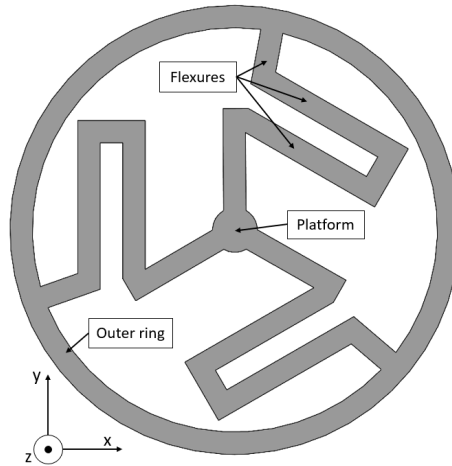


Figure 2.1: An OPS example to show the name definitions further used.

2.2.1. CAD DESIGN

Each of the selected OPSs has been remade in CAD. These Designs can be seen in figure 2.2. The thickness of these designs is chosen to be $100\mu\text{m}$, a size widely available for laser cutting. For the outer dimensions a size of 10mm was chosen, the size of a small coin battery. The overview of all the OPSs can be seen in figure 2.2. The dimensions of all flexures are estimated from the original design images.

2.2.2. COMSOL ANALYSIS

The CAD models are all analysed using COMSOL to make an estimation of the stiffness. For this the material of steel is applied to all models. The outer ring is fixed and a displacement is applied to the center platform of each OPS. The force is then measured and a estimation of the stiffness of each OPS can be made. Two different analysis were applied. The first analysis was a displacement of $10\mu\text{m}$. The force required for this displacement was used to calculate the stiffness. This small displacement gives an indication of the stiffness in the linear regime. The second analysis a bigger displacement of $500\mu\text{m}$ was applied. For this bigger displacement non linear geometries were accounted for in COMSOL.

With the same constraints as in the COMSOL model an estimation of the frequency of the first eigenmodus can be made. This not only allows insight into the dynamic response, but also shows how these springs deform.

2.2.3. DOF ANALYSIS

From the modal analysis also insight can be gained into the degrees of freedom (DOF) of the system. This is used to estimate the main DOF of the center platform. Different DOFs can be present in the system but focus is put on the out-of-plane DOFs of the center platform. The axis directions can be noticed in figure 2.1. Because the DOFs are really dependent on each design, the analysis is done for each class. The systems which are not fully supported from 3 or more sides usually have a lot more DOFs compared to the other designs.

2.3. CLASSIFICATION

A classification is made based on the flexure configuration, shown in figure 2.3. The OPSs are referenced based on the labels used in figure 2.2. Multiple configurations patterns were defined and the OPSs are classified according to their flexure topology. Categories are split up in straight and curved flexure designs.

1: OPS - Folded pattern - Tangential

An example of this configurations is OPS-nr.1. The flexures are folded and support the middle platform in a tangential configuration. This results in a very compact design because the flexures can be folded multiple times.

2: OPS - Folded pattern - Radial

This category supports the platform in a radial configuration, like shown in OPS-nr. 20. Designs which make use of curved flexures has not been found in literature. In [24] the difference between the tangential and the radial design is compared. It showed for these patterns the same linear compliances but different rotational compliances.

3: OPS - Folded pattern - Other

This category describe all other possible configurations that are making use of a folded flexure. OPS-nr.9 is an example of this category, where the design consist of 2 folded flexures resulting in an unstable system. OPS-nr.11 shows a folded pattern design. However, this configuration has connected all flexures, creating multiple rings.

4: OPS - Circular pattern

The designs in this category support the platform in a circular configuration. An example of this category is OPS-nr.5. These designs can be very low stiffness because the flexures can circle around the platform, allowing for long flexures. A more difficult problem elaborated in [34] is the fact that the flexures not only suffer bending, but are also torsionally loaded.

5: OPS - Straight pattern

These design patterns support the platform directly with straight flexures. These designs usually result in a very high stiffness design, because the flexures are usually comparatively short in length. While OPS NR 12 could also be classified in the circular group, it is put in this group because of the almost straight flexures.

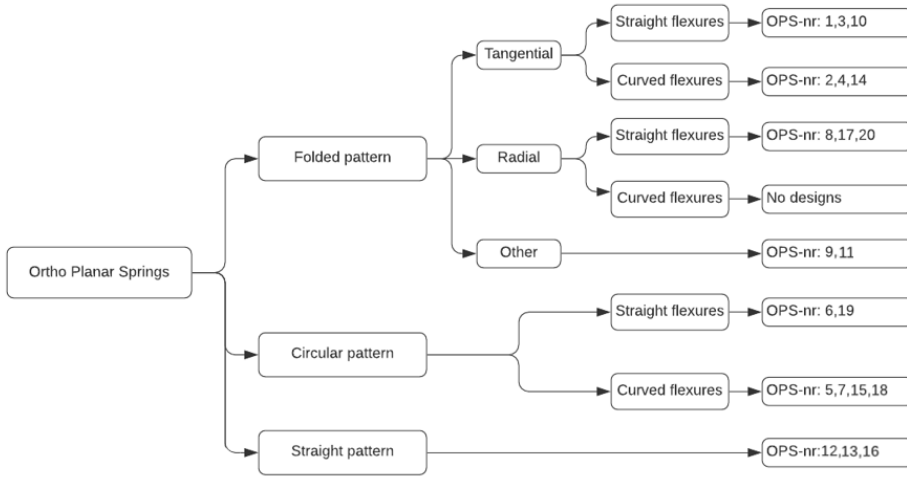


Figure 2.3: Classification of OPS based on flexure topology. The folded pattern class is split up because of the wide array of variations possible.

2.4. RESULTS

Figure 2.4 shows the results of the stiffness analysis explained in the methods section. The two bars at 6 and 19 are empty because the model could not be solved by COMSOL, due to non convergence in the non linear geometries.

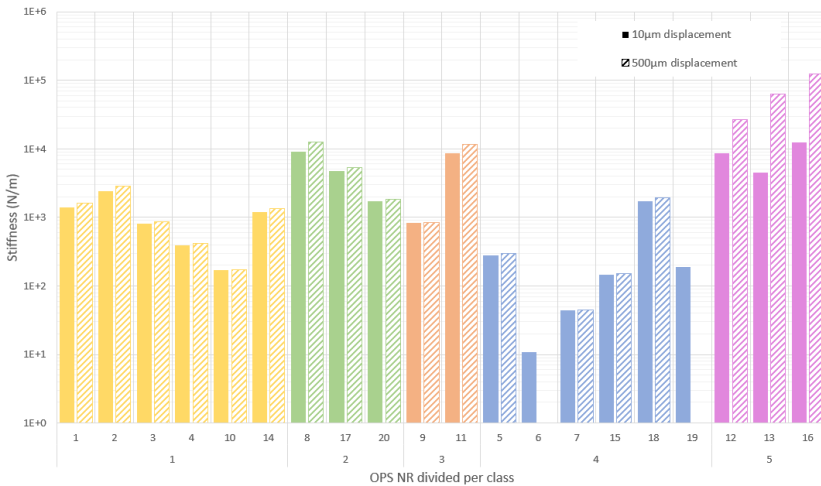


Figure 2.4: Stiffness of each OPS, divided per class. Displacement is measured with COMSOL for a smaller and bigger displacement, including non-linear geometries

In figure 2.5 the eigenmode frequency of each OPS is shown. The frequency shown is for the first eigenmode.

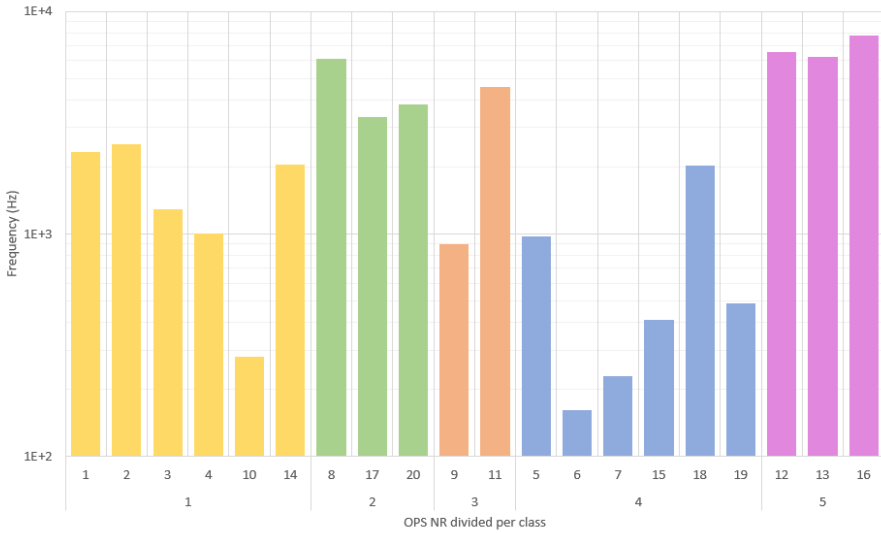


Figure 2.5: First eigenmode frequency of each OPS, split up in classes. Measured with COMSOL

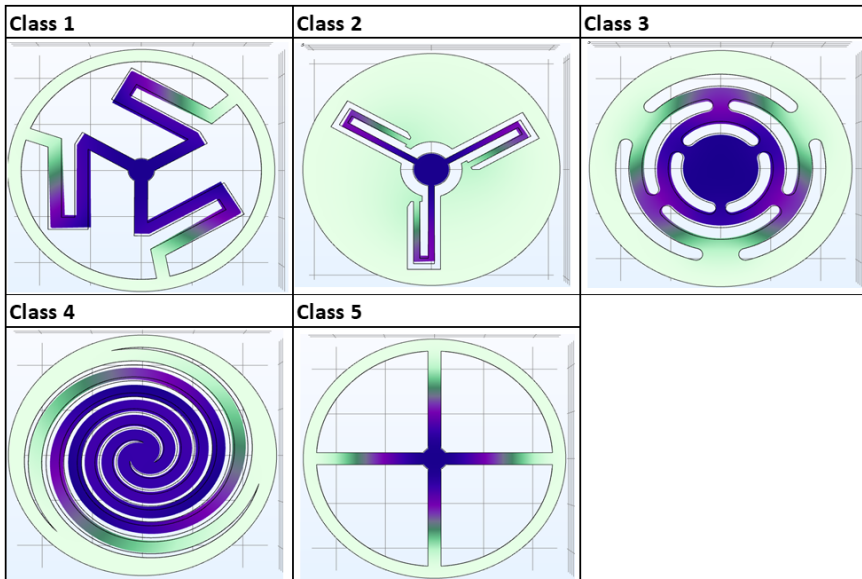


Figure 2.6: First eigenmode of an example spring from each class. The darker the colour the higher the displacement. The black contour lines show the spring in undeformed state.

Each class mentioned in section 2.3 DOF is shown in table 2.1.

Class of OPS	DOF
1: Folded - Tangential	disp_Z
2: Folded - Radial	disp_Z
3: Folded - Other	disp_Z
4: Circular Pattern	disp_Z+rot_Z
5: Straight Pattern	disp_Z

Table 2.1: Main degrees of freedom from each class

2.5. DISCUSSION

2.5.1. STIFFNESS ANALYSIS

The OPS stiffnesses are shown in figure 2.4. Each stiffness is mostly dependent on the design choices made but remarks can be made for some classes.

Class 1, the folded pattern tangential, shows relatively low stiffnesses. The folded pattern allows for long flexures and because the flexures are placed tangential to the center platform most of the space can be used. Increasing to bigger displacement does not seem to have much impact, these designs allow for a larger range of motion, compared to other classes.

Class 2, the folded pattern radial, still have relatively high stiffness. The folding of this configurations happens radial to the center platform. This gives big restrictions in the space available for the designs, because this configuration needs space between the center platform and the outer rings. For bigger displacements the designs do show a higher stiffness, due to the relatively short flexures.

Class 3, folded pattern other, no real conclusions can be drawn. Mostly because this group consist of different configurations.

Class 4, the circular pattern design, results in mostly the lowest stiffness. The flexures being placed in a circular way, allows for long flexures resulting in the lowest stiffnesses. These long flexures also allow for bigger displacement, thus barely an increase in stiffness can be noticed for larger displacements.

Class 5, the straight pattern, has the highest stiffnesses. This was to be expected because the straight configuration results in short flexures with high stiffnesses. For most designs the stiffness increases only slightly with the larger displacements and including geometric non linearities. However for class 5, the straight pattern, the stiffness does increase significantly. This is due to the design of these OPS not allowing large motions. To allow this motion the system not only bends but also needs to stretch. For VEH purposes this would result in a very limited motion in these designs.

2.5.2. EIGENMODES

The exact values of the frequencies are not that important. For VEH purposes lower frequency's are desired. This frequency can be lowered by the addition of extra masses to the platform, as shown in [16]. The frequencies for the first eigenmode look very much like the stiffness graph shown in figure 2.4, as expected, because the eigenmode is directly related to the stiffness. The lowest frequency's can be seen in the class 4.

2.5.3. DOF ANALYSIS

As Parise et al.[10] defines: A stable platform can be defined as a platform that can not easily move outside its prescribed direction. In the DOF analysis the springs containing 3 or more legs were only used. Because any less than this would result in an unstable platform which is not desired because it would create planar movement and could result in a collision within the system.

All classes show the desired DOF, the displacement in the z-direction. But class 4, the circular patterns, have a combined displacement with a rotation of the platform. This need to be accounted for, because anything fixed to the platform will also have to rotate. It would also result in torsional stresses which could increase fatigue in the system [10].

2.5.4. STRAIN

To apply piezo energy harvesting big strains are desired in the OPS. The deformation of a guided flexure is schematically shown in figure 2.7, with the high strain parts marked in red. Classes 1, 2 and 3 are all folded pattern designs, which consist of multiple short flexures due to the formation of intermediate platforms. Class 4, the circular pattern, consists of one flexure which makes the piezo energy harvesting more complex. In Deterre et al.[34] a method for piezo patterning is proposed, that would reduce this problem by tactical placement of the electrode connections.

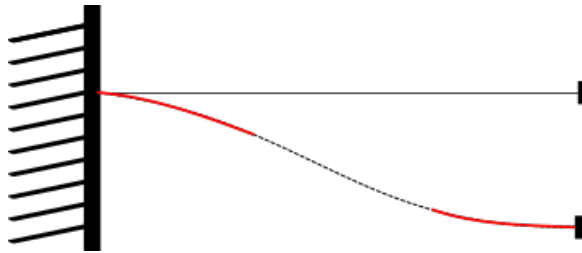


Figure 2.7: Schematic view deformation of a guided beam. High strain areas are marked with the red line.

2.6. CONCLUSION

A literature review of 20 Ortho Planar Springs (OPS) has been performed. A classification is proposed based on flexure configuration resulting in 5 classes. Each spring was re-made in CAD en analysed using COMSOL. The stiffness and frequency of the first eigenmode was computed. We have found the stiffness of the OPS design can be lowest when using either a folded or circular pattern. To use the springs with low frequency vibrational energy harvesting (VEH) masses should be added to the platform to allow the frequency of the first eigenmode to drop. The degrees of freedom (DOF) of each class is also analysed and showed the circular pattern designs have a disadvantage due to their DOFs having a combined rotation and displacement. The strain distribution over the classes is compared, where the folded pattern classes show an advantage due to the multiple flexure designs. All this combined showed insight in different OPS classes in literature, which could be used in future VEH designs.





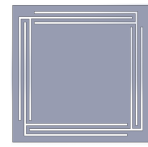


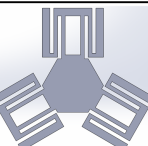




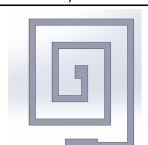
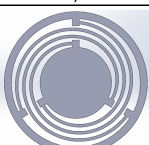


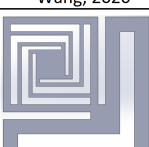



Class 1: Folded Pattern tangential	1	2	3
	Dothe, 2016	Han, 2016	Qiu, 2016
			
	4	10	14
	Nguyen, 2004	Teichert, 2013	Smal, 2008
			
Class 2: Folded Pattern radial	8	17	20
	Smal, 2006	Hao, 2017	Qui, 2016
			
Class 3: Folded Pattern other	9	11	
	Smal, 2006	Smal, 2006	
			
Class 4: Circular Pattern	5	6	7
	Tian, 2020	Hu, 2011	Tao, 2015
			
	15	18	19
	Deterre, 2013	Cheng, 2013	Wang, 2020
			
Class 5: Straight Pattern	12	13	16
	Smal, 2006	Smal, 2006	Graipaspong, 2018
			

Figure 2.2: Overview of all Ortho Planar Springs used. Each OPS is remade in CAD with the same outer dimensions. The OPS are already divided in the classes explained in section 2.3. The models are also used for COMSOL analysis.

3

DESIGN OF A BI-STABLE IMPACT BASED FREQUENCY UP CONVERTER

This chapter describes the energy harvester design made and used for this research. This design is a Bi-stable Impact-based Snap-through frequency up converter (BISup). It discusses the designs choices made and how it works.

3.1. SCHEMATIC MODEL DESIGN

To create an energy harvester design a schematic was created, shown in figure 3.1 This energy harvester design is based on a double mass-spring-damper system. In this model the m_1 represents the low frequency oscillator. The m_p represents the high frequency oscillator.

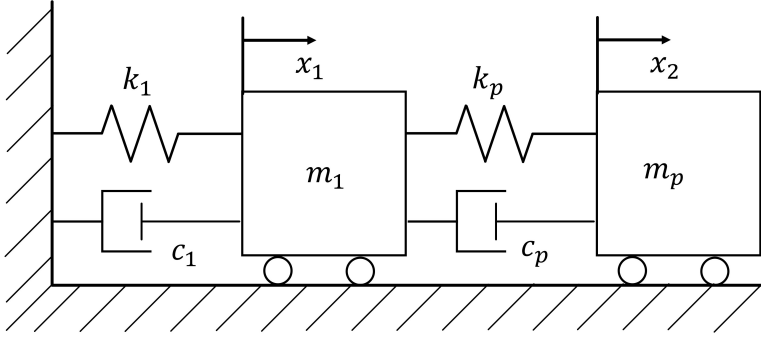


Figure 3.1: The energy harvester design represented as a double mass spring damper system. This design is based on a frequency up converter where the m_1 is the low frequency oscillator and the m_p is the high frequency oscillator.

This model can be modelled with the equations shown in equation 3.1.

$$\begin{aligned} m_1 \ddot{x}_1 &= -k_1 x_1 - c_1 \dot{x}_1 + c_p (\dot{x}_p - \dot{x}_1) + k_p (x_p - x_1) \\ m_p \ddot{x}_p &= -c_p (\dot{x}_p - \dot{x}_1) - k_p (x_p - x_1) \end{aligned} \quad (3.1)$$

Each of the mechanical parameters depend on the design chosen. This model can be implemented in MATLAB to simulate the behaviour of the system. The design choices for each element are discussed in this chapter.

3.2. BI-STABLE IMPACT-BASED SNAP-THROUGH FREQUENCY-UP CONVERTER

The full EH design is shown in figure 3.2. The design is made bi-stable with the flat flexure clamped between curved frames. This functions as the low frequency oscillator of this design. A piezoelectric beam is added on the mass block to function as high frequency oscillator. The snap through behaviour of the bistable flexure can create an impact like vibration on the high frequency oscillator. This design is called the Bi-stable Impact-based Snap-through frequency up converter (BISup). The short beam is made from piezoelectric material. When this beam starts vibrating power can be generated and captured.

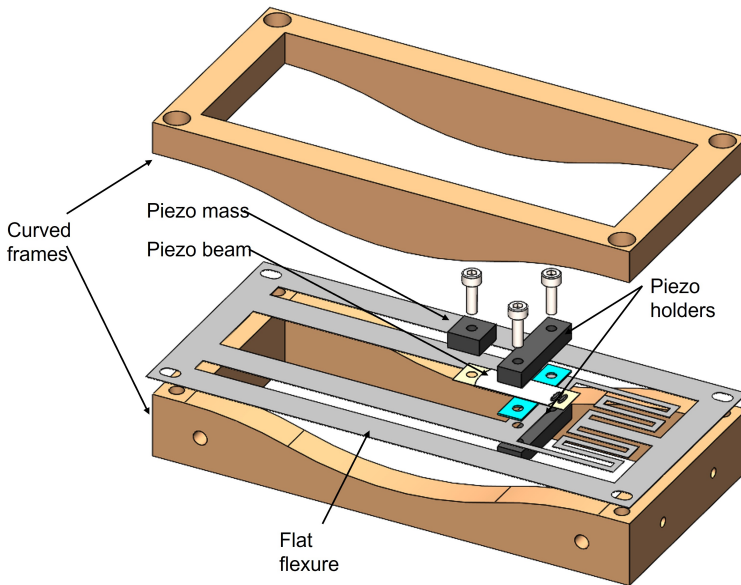


Figure 3.2: The Bi-stable Impact-based Snap-through frequency Up converter (BISup). This design consist of curved frames, which are used to apply a preload to the flat flexure. On the flat flexure a piezo beam with mass is added using the piezo holders. There is also a thin film, shown in blue, with a small cut out to better grip the piezo.

Every important part of this design is further explained in the sections below. First the flat flexure which functions as the low frequency oscillator is discussed. Next the design of the piezo beam which is integrated in the high frequency oscillator is discussed. The piezo is touched on and all its properties are measured and calculated. The design goal for this thesis is discussed next and some initial designs are shown and classified.

3.2.1. LOW FREQUENCY OSCILLATOR

The low frequency oscillator (LFO) consists of a flat flexure, shown in figure 3.3, being preloaded by the use of curved frames. The curved frames clamp the flat flexure and thus apply a deformation to the edges of the flat flexure. This results in the endpoints

(shown in red) getting closer together and thus applying a preload. The preload distance can be calculated with arc formulas, shown in appendix C.

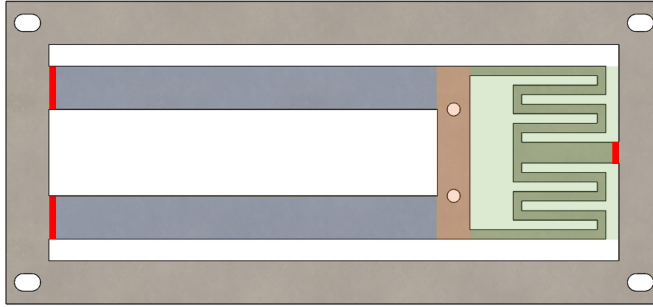


Figure 3.3: The flat flexure used. In blue the leaf spring arms are shown. The orange part shows location of the added mass. The green part shows the folded flexure area. The parts in red show the connections with the frame

In figure 3.3 multiple sections can be noticed. First, in blue, the leaf spring arms are shown. In orange the mass block part is shown. This is the part where maximum displacement occurs and mass can be attached. In green the area of the folded flexure is shown. This is the folded pattern used. The red marks show the outer edges which are pushed closer by the curved frames.

The preload results in a bistable system. The two stable positions are schematically shown in figure 3.4. In this figure the block part represents the mass block which can be added.

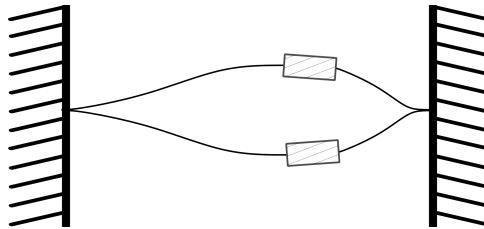


Figure 3.4: Schematic representation of the system after preloading. Two possible positions are shown in which the system is stable. The block represents the mass block or other systems added.

3.2.2. HIGH FREQUENCY OSCILLATOR

The high frequency oscillator (HFO) used is shown in figure 3.5. This part is added on top of the mass block part of the low frequency oscillator. The HFO consists of 2 blocks which clamp a piezo beam. In the fabricated design these blocks are made from PMMA. The piezo beam is clamped together with the orange part of the flat flexure shown in figure 3.3. Because the piezo is clamped onto the bi-stable flat flexure, a thin blue film is added to ensure electrical isolation between the piezo beam and the bi-stable flat flexure. A tip mass is also added to adjust the resonance frequency as desired.

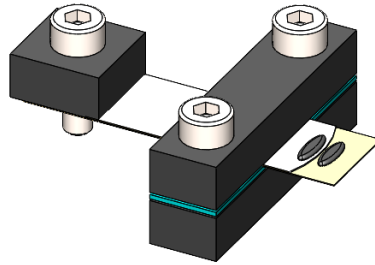


Figure 3.5: The high frequency oscillator. Consist of 2 blocks to clamp the piezo to the flat flexure, and another block to add mass to the tip of the system. A thin blue layer is added to ensure electrical isolation between the piezo beam and the bi-stable flat flexure.

The HFO starts resonating when the LFO switches from stable points and an impact like vibration occurs. The piezo beam choice and performance is discussed in the next section

3.3. PIEZO

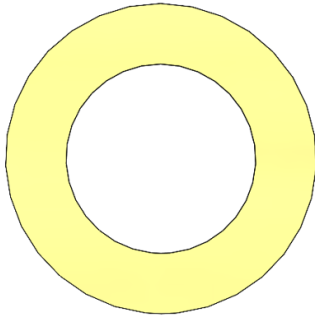
3.3.1. BI-MORPH PIEZO

This section describes the different piezo designs used, also the performance and mechanical behaviour of the piezo implemented as the HFO. Initially a bi-morph piezo-electric cantilever was used as transducer in this design. The material of this beam is the PZT508. The strip is of rectangular with a width of 4mm and a thickness of 0.8mm. The length could be manipulated by clamping the piezo at different lengths. This strip was not used in the final design because of its stiffness which resulted in a high eigenfrequency. This design choice is further discussed in chapter 5

3.3.2. PIEZO BUZZER

The next alternative was a piezo buzzer. This buzzer can be lasercut to the desired shape. This allows for easy modification of the piezo and also the HFO. Another advantage to using this buzzer is the low stiffness, which results in a low eigenfrequency. In figure 3.6 the original piezo buzzer is shown and next to it the laser cut design used. The piezo buzzer is the FT-41T-1.0A1-478 Ceramic piezo buzzer. This buzzer consists of a brass surface with a diameter of 41mm. A ceramic layer with a diameter of 25mm is attached on top of this brass layer.

For the use of this piezo in the HFO the design is lasercut as shown in figure 3.6b. The design consist of 3 holes to be able to mount different size weights to the system. The two soldered area at the bottom allow for the electrical connections to the system.



(a) The original piezo buzzer used. This buzzer consist of a brass bottom layer (in yellow) with a ceramic piezo layer attached on top (in white).



(b) Laser cut buzzer design with soldered connection points. The three holes at the top of the piezo allow for easy tip mass addition.

Figure 3.6: The used buzzer (FT-41T-1.0A1-478) shown in (a) is laser cut to make (b). The laser-cut design consist of 3 holes for possible mass addition.

3.4. FABRICATED DESIGN

The fully fabricated BISup is shown in figure 3.7. This design was mostly used to get a feeling on the behaviour of the system and gain insight in the movement of the BISup. In this figure electrical wires can be noticed, these wires are later fixed along the big leaf springs. They are given enough leeway to not affect the BISup's behaviour. However, when using this design the lead stiffness should be considered.

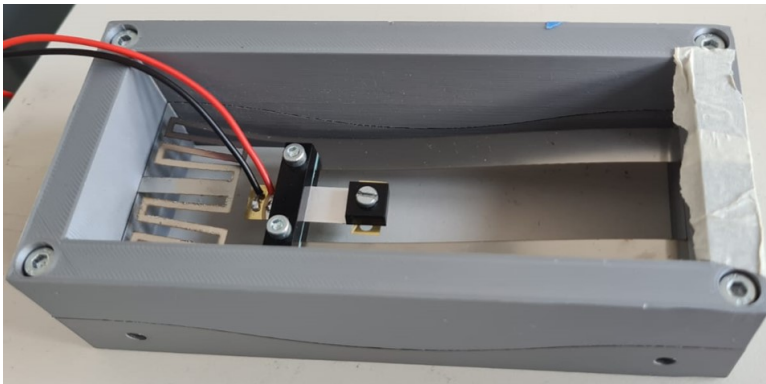


Figure 3.7: The fully fabricated BISup design. This design was used for initial tests on the behaviour of the system.

4

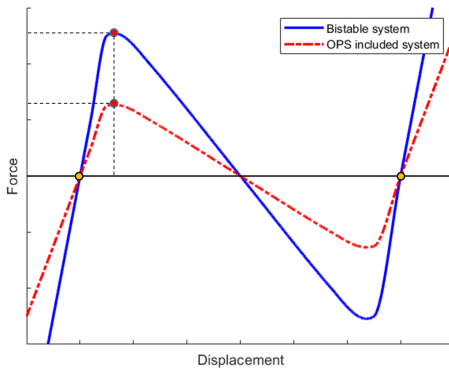
ORTHO PLANAR SPRING INSPIRED DESIGN AND TUNING

This chapter explains the design of the ortho planar springs for the folded flexure part. Multiple designs are simulated in ANSYS to get insight in the mechanical behaviour. These designs are compared to each other to find the best design for its purpose.

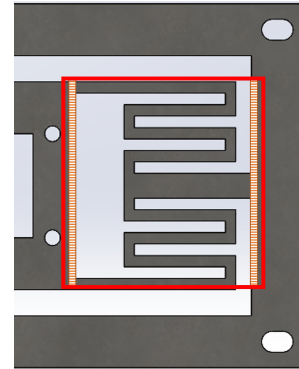
4.1. DESIGN GOAL

The BISup design was used to do initial tests on the system and to get insight in the use of the folded pattern in the bi-stable system. The switching force of a bi-stable system is the maximum force required to switch the bi-stable system from one stable state to the other. From this device it was noticed the switching force required is way lower compared to a design without the folded pattern. From this a design goal could be made. A device with low switching force will start to switch at lower accelerations. A design goal could be made. The focus for this design goal lies on adjusting the bi-stable system. In figure 4.1a the force deflection goal of the design is schematically shown. The main goal is to lower the switching force needed, allowing for switching at lower accelerations. It is important to work in the same amount of space in each design. Therefore figure 4.1b shows a red box which shows the size of the design area.

4



(a) The force deflection goal of the OPS included design. The main goal of designing is lowering the switching force. The red points show the maximum switching force and the yellow dots show the stable equilibrium points



(b) The design area is shown in the red box. In here the design can be made. The striped line show the places were the flexure can be connected to the frame and the rest of the system

Figure 4.1: In (a) the design goal for the bi-stable system is shown. In (b) the boundary condition on design space is shown.

4.2. DESIGN CONCEPTS

Within the requirements and boundary conditions mentioned different designs could be made. Multiple ortho planar spring were used to generate different designs. These design schematically show a plethora possibilities for the folded flexure design.

From the selection of designs made a classification can be executed, this can be used to reduce the amount of designs used for analysis. The classification made is shown in figure 4.2.

The designs are initially divided in 2 main groups; The folded and non-folded designs. Almost every group is in the end subdivided in single and multiple fold. These division are made to show designs with multiple folded flexures.

NON-FOLDED

These are designs which do not contain a folded flexure. The straight connection design is a great example of this group. The straight design is already widely used for bi-stable systems and creates a simple design. The short flexure makes the stiffness relatively high.

Also in this group are non-straight designs. These designs rely on flexures that are not folded but do have a flexure which bends and also twists.

FOLDED

The folded designs main principle is the implementation of a folded flexure. The introduction of the folded flexure should allow for longer flexures, this should lead to lower stiffness, and thus a lower switching force.

The first interesting sub-group from this group are the folded-horizontal class. This group consists of folded flexures which connect parallel to the big leaf spring. A great advantage of this group are the long folded flexures. These should allow for lower switching forces. The next sub-group are the folded-vertical springs. Like the horizontal group make use of a folded flexure but this time orthogonal to the big leaf spring. Finally a mix group is added which consist of a combination of the two other groups. This group makes the design very complex and this results in a stiff design because the flexures have no room to bend.

Not Folded	Straight		Single connection	
			Double connection	
	Non Straight		Single symmetric	
			Double symmetric	
Folded	Horizontal	Single symmetric	Single fold	
			Multiple fold	
		Double symmetric	Single fold	-
			Multiple fold	
	Vertical	Single symmetric	Single fold	
			Multiple fold	
		Double symmetric	Single fold	
			Multiple fold	
	Mix			

Figure 4.2: The designs made classified in the different classes. 2 main groups were created; the folded and not folded designs.

4.2.1. DESIGNS FOR ANALYSIS

From this design tree the most interesting classes are further analysed. The selected designs are shown in figure 4.3. The main classes of interest are; The straight designs, the folded-horizontal designs and the folded-vertical. These are interesting because the other designs consists of combinations of these groups. Also chosen are 2 more complex variations of the simple designs. These designs are included to gain insight on the effect of multiple folds.

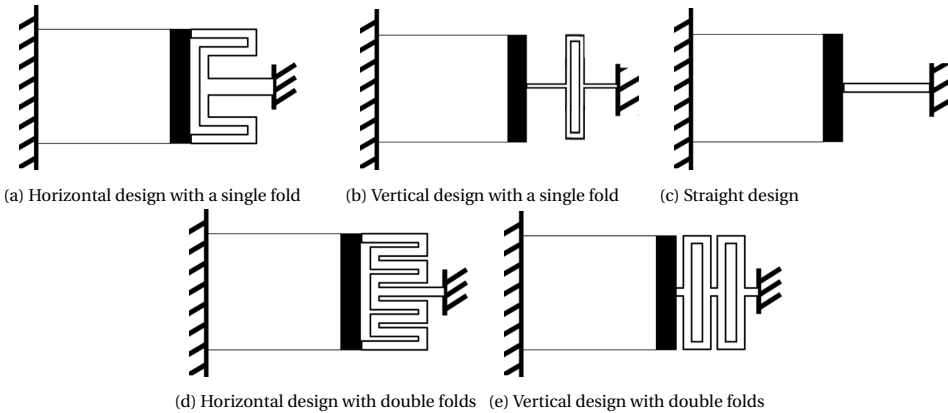


Figure 4.3: The chosen designs from the designs tree shown earlier. These designs are further analysed in ANSYS. The designs of a,b,c are chosen as they represent the simplest designs, and can be used to derive the other designs. c,d are added as they represent a more complex version of a,b.

4.3. ANSYS MODEL SET-UP

The force-deflection (FD) behaviour of the flat flexure is modelled using ANSYS. ANSYS is a finite element model software used for solving mechanical problems. The material used is spring steel (with $E = 190\text{GPa}$, $\rho = 7.82\text{g}\cdot\text{cm}^{-3}$). In ANSYS, the system is modelled as a system of nodes and beam188 elements. The long leaf springs are divided in 40 elements. The mass block is created as a beam element with a thickness of 10mm and divided in 2 elements as this part will not significantly deform. For the folded flexure the different beams are divided in 20 segments for longer arms and 10 for shorter arms. The elements are modelled as thin lines meshed with beam elements. Because of this, overlap can occur in the modelling without issues. The end point of leaf springs are fixed. The end of the folded flexure is preloaded by adding a small displacement equivalent to the displacement generated by the curved frames. This displacement is 1.8mm for all designs.

A displacement is applied to the centre of the mass block and the reaction forces are measured. Non linear stabilization was applied to make sure the snap through behaviour of the system would not be an issue. The value of stabilization added is $1e5$, this stabilization is added because of the uncontrolled snap through occurring in this system. For all ANSYS model the base is kept identical and only the folded flexure part is adjusted according to the part designed.

4.4. DESIGN SIMULATION

Each design is made in ANSYS, where the only difference in modelling is made in the folded flexure part. To be able to compare the designs the width and thickness of all flexures are kept equal. To compare the different designs to each other the flexural rigidity is used. The flexural rigidity is the force required to bend. The ratio of flexural rigidity is used to easily compare designs, even in further research. The flexural rigidity left of the mass block is compared to the folded spring part right of the mass block, shown in equation 4.1.

$$EI_{\text{right}} = EI_{\text{left}} \quad (4.1)$$

In this equation E is the Young's modulus. The I in this equation is the area moment of inertia. For a rectangle cross-section this is given as equation 4.2.

$$I = \frac{1}{12}wh^3 \quad (4.2)$$

In this equation w is the width of a flexure, and h is the height or thickness of a flexure.

Each model was designed in ANSYS and then the force deflection behaviour of each system could be simulated. First each class was compared to the original straight design. For the initial simulations the ratio flexural rigidity right:left is taken as 5:1. This is done by making the left flexure width 5 times the flexure width of the right side.

4.4.1. HORIZONTAL DESIGN

Both the single horizontal and double horizontal flexure are simulated in ANSYS. The generated graph of the force deflection behaviour is shown in figure 4.4.

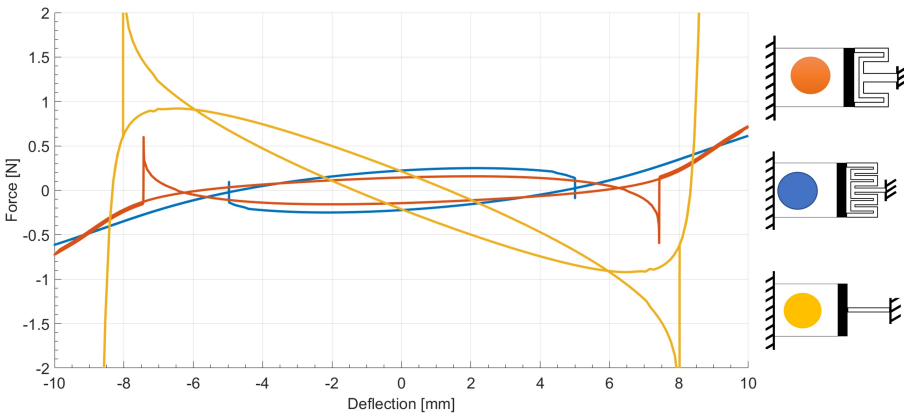


Figure 4.4: The force deflection graph generated of the horizontal flexure designs. The original straight design is also shown as a comparison. The high peaks occur after snap through in the simulation and does not occur in reality.

In this graph some peaks are visible, these peaks occur because of the software trying to simulate the snap through of the system. This does not occur in reality and can therefore be ignored. The original design, shown in yellow, behaves as expected non-linear and bistable. The stable points occur at $\pm 8.5\text{mm}$. When compared with the other 2 designs a significant difference can be noticed. First the peak force needed for snap through is lowered. Second, the distance between the stable points is also lowered. Thirdly, the stiffness of the design in a stable point is also significantly lowered. While these effects can be expected when trying to flatten the FD curve, something else can be noted. The double horizontal variant seems to need a higher force for snap through to occur. This is unexpected because using more flexure should lower the stiffness and thus the overall force necessary.

4.4.2. VERTICAL DESIGN

The force deflection of the vertical designs compared to the straight designs is shown in figure 4.5. To be able to solve these designs the stabilization was increased to $1e6$.

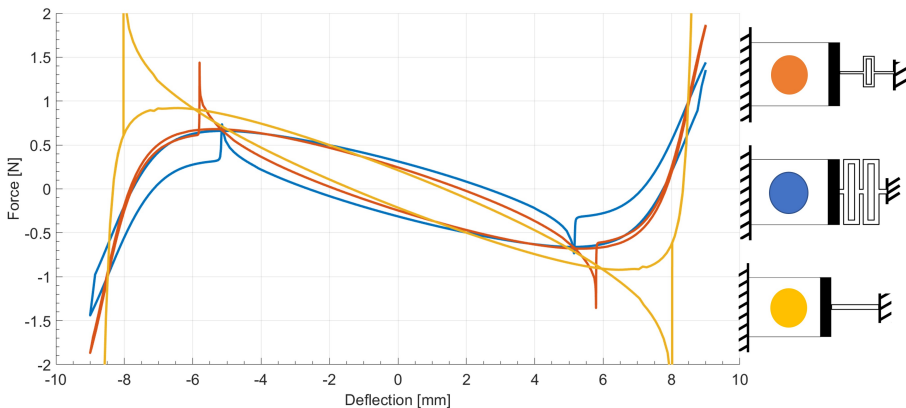


Figure 4.5: The force deflection graphs of the vertical flexure designs, compared with the original straight design. The high peaks can be ignored and appear to the snap through behaviour in the software. The hysteresis of the vertical double design can be explained due to the high stabilization required for computing the force deflection

Again high peak forces can be noted. These forces occur due to the solver handling the snap through. These peak forces do not occur in reality. A lot of hysteresis is visible for the blue line, the double vertical design. This is present because of the ANSYS software requiring a high amount of stabilisation to be able to compute the force deflection behaviour. It can be noticed that these force deflection do lower the snap through force required, however significantly less compared to the horizontal design. A reason for this could be the fact that the vertical flexures are shorter due to the space available.

4.5. PARAMETER STUDY

The designs presented are all presumed to have the same flexural rigidity ratio. However, to check if the thickness of the flexures affects the behaviour, a parameter study is also performed. In these parameter studies the flexural rigidity from either side is altered to observe the changes to force deflection graphs. The parameter study is applied to the designs shown in 4.3a, 4.3b and 4.3c. The horizontal single design had the best performance in the initial force deflection simulation. The straight design is also simulated because this is a more conventional design. The vertical single design had some problems computing and needed a lot of extra stabilization to compute. This caused the hysteresis to increase greatly and the results are thus unreliable. The graphs are shown in appendix A.

4

4.5.1. HORIZONTAL SINGLE

The horizontal single design shown in 4.3a. By changing the width of the flexures the flexural rigidity can be directly altered. The force deflection is measured for different widths and results in the graph shown in figure 4.6. The legend shows the values of flexural rigidity in Nm^2 for each force deflection.

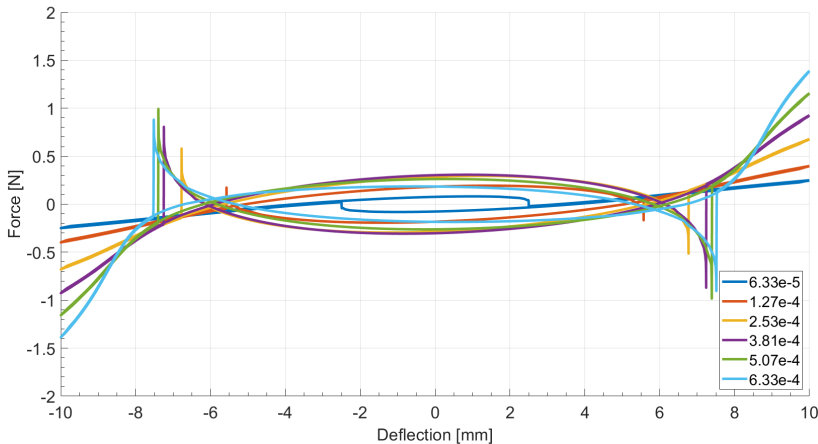


Figure 4.6: The parameter study on the horizontal folded flexure. The width of the flexures is adjusted and the resulting flexural rigidity is shown in the legend in Nm^2 . For the blue line, with the lowest flexural rigidity, the force deflection behaves almost linear.

This parameter study gives insight in the effect of the flexural rigidity on the behaviour of the system. When the flexural rigidity is low, as seen in the blue line, the system almost behaves linearly. Something else to notice is increasing the flexural rigidity increased the snap through force, until after increasing it more the force seem to lower again. To explain how this lowering occurs further research into how the solver simulates is necessary.

The stable point locations seem to move further away from each other with increasing flexural rigidity. The stiffness in these stable points seem mostly the same. However,

the stiffness past this point gets significantly higher for increasing flexural rigidity. This is to be expected because the system at this point is trying to stretch the material and a bigger flexural rigidity requires more force to stretch.

4.5.2. STRAIGHT SINGLE

The straight single design shown in 4.3c. The same study as before is done, where the flexural rigidity of the right side of the system is altered to investigate what happens to the force deflection behaviour. The force deflection graph is shown in figure 4.7. The legend again shows the flexural rigidity of the folded flexure in Nm^2 .

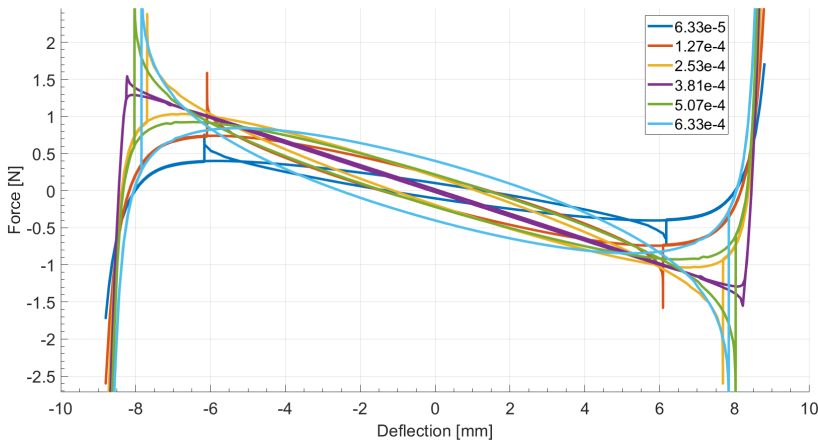


Figure 4.7: The result of the parameter study, where the flexural rigidity of the straight designs is altered by changing the width of the flexures. The legend shows the flexural rigidity in Nm^2 . Changing this does not seem to affect the behaviour significantly.

The force deflection behaviour result is a bit counter intuitive. Initially the snap through force increase with an increasing flexural rigidity. But then snap through force seems to lower again for increasing flexural rigidity. To explain these phenomena further research is necessary. The stable point locations of the system seem barely effect as well as the stiffness in this point which mostly stays the same. So changing the width of straight designs does not affect the mechanical behaviour significantly. The hysteresis in this loop does seem to get bigger with increasing flexural rigidity.

4.5.3. RESULTS

The results of the parameter study are difficult to oversee. To better compare the data, different factors are compared. The snap-through force required is plotted against the flexure width, shown in figure 4.8. The snap-through force for the straight design is always bigger compared to the horizontal folded design. Something else to note is both designs snap-through force seems to increase with the width. But around halfway the snap-through force starts to lower again. A reason for this could be the snap-through occurs on the other side of the mass at the leaf springs. However, to be sure about this

more research is necessary.

In figure 4.9 the range of motion for each width is plotted. The range of motion for the horizontal designs seems to increase with the flexure width. This is as expected because the wider flexures get pre stressed and more stress results in more range. For the straight pattern however, the range of motion increases at first and then decreases. This could again be explained by the snap-through occurring in a different way resulting in the lower range. The straight design range of motion does change, but not by any significant amount

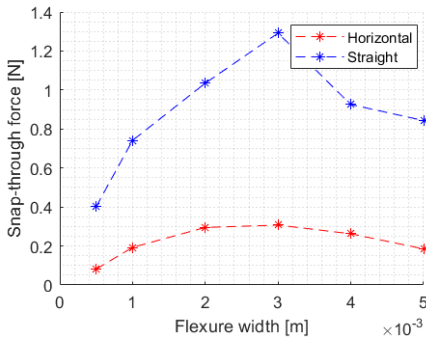


Figure 4.8: The snap-through for both designs shown as function of the flexure width.

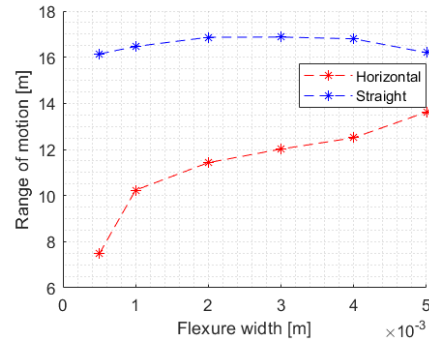


Figure 4.9: The range of motion for both designs as function of the flexure width.

4.6. COMPARISON

To easily compare the 3 main designs to each other, different aspects of the force deflection of each design is noted. All of these results are shown in table 4.1. Each design in this table uses the same flexure width of 2mm. First the switching force of the designs are given. As explained in section 4.1, this is the maximum force necessary to switch a bistable unit from 1 stable point to the other. Lowering this force would result in switching at lower accelerations. This could be of use in the design of energy harvesters and improve their performance. Second the switching range is given. This is defined as the distance between stable points. In this table this is unit is given in mm. Finally the stiffness in a stable point is given. This stiffness is important as the designs will vibrate around the stable points.

SWITCHING FORCE

The switching force of the horizontal designs is the lowest. This was to be expected from the earlier force deflection curves shown. The reason why the force is lowest is the design allowing for the longest flexures. The straight design is the stiffest. This design has just 1 flexure which makes it have the highest stiffness. The vertical design lies inbetween the other two. This is due to the design space not allowing for optimal flexure length. So while the design has a lot of flexures, these flexures are very restricted in their length and thus a bit stiff.

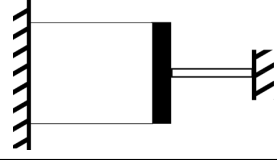
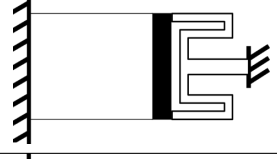
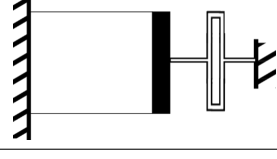
Design	Switching Force [N]	Switching Range [mm]	Stiffness in stable point [N/m]
	1.035	16.86	3999
	0.295	11.43	96.97
	0.795	15.85	1513

Table 4.1: A table showing different characteristics of the force deflection curves of the 3 designs. The switching force is shown in newton. The distance between the stable points is called the switching range. And finally the stiffness in the stable points is given. Each design is rated with flexure having a width of 2mm

SWITCHING RANGE

The values of the switching range for each design shows there is a trade off between the switching force and the switching range. While the horizontal design has the lowest switching force it also has the lowest range. This range can be of influence in the design choices made. A lower switching range could influence the impact generated when switching.

STIFFNESS IN STABLE POINT

The stiffness in the stable points is also important for comparing. This stiffness gives insight in how the system will behave after switching. When switching a bigger impact will be present when the stiffness in the stable point is higher. The straight design has the highest stiffness, as expected, because it contains the least flexures with overall the shortest length. The horizontal design has a very low stiffness in its stable point. Again this is due to the long flexures allowing for this low stiffness.

4.7. CONCLUSION

From the different designs made each has its advantages. However, for the intended purpose a lower snap-through force is very important. The horizontal design allows this lowering and is thus the best for this use case. It should be noted that the lowered stiffness in the stable point could lead to a lower impact vibration, but further research is necessary.

5

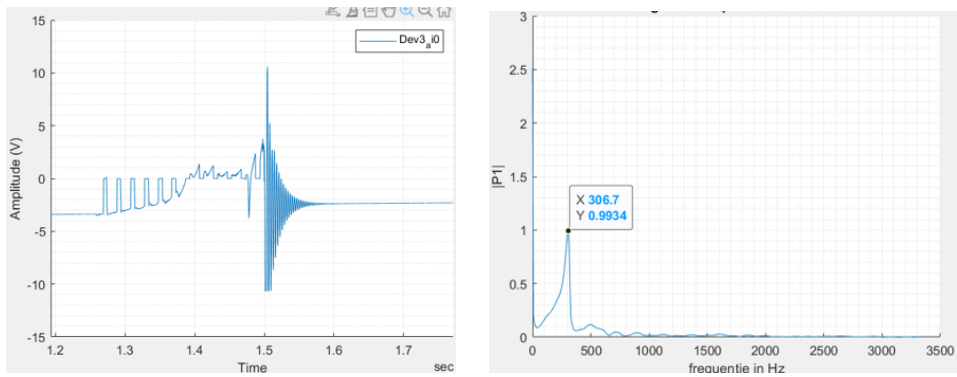
EXPERIMENTAL VERIFICATIONS

This chapter shows all the experimental verifications performed. The dynamic model is made and simulated using MATLAB.

5.1. BI-MORPH PIEZO

5.1.1. EIGENFREQUENCY MEASUREMENT

The piezo beam needs to be resonating in its eigenfrequency for the best performance. However, if this frequency is very high the frequency up converter has trouble exciting this eigenfrequency. To get an estimate of the eigenfrequency of the bi-morph piezo beam an experiment is executed. The bi-morph piezo beam is fixed and one of its outputs is measured using a national instruments data acquisition box (NI USB6211). The beam is then manually plucked and the voltage output is measured, the resulting graph can be seen in figure 5.1a. To get an estimate of the eigenfrequency a fast fourier transform (FFT) is performed. The marked area shows the part of the graph used for the FFT. The resulting single sided spectrum is shown in figure 5.1b. This give a value of the eigenfrequency of 306Hz. The frequency being so high resulted in the piezo beam not oscillating when implemented in the energy harvester design. This is further explained in appendix B



(a) The area used for the fit is the part where the piezo is freely resonating.

(b) Applying a fast fourier transform gives us the main resonance peak.

Figure 5.1: The piezo is manually plucked, the signal shown here in (a) is the voltage measured over the bi-morph piezo. In (b) a FFT is executed on this signal and the single sided spectrum is shown. The eigenfrequency for this beam lies around the 306 Hz.

5.2. LASER-CUT PIEZO BUZZER

5.2.1. EIGENFREQUENCY MEASUREMENT

The eigenfrequency of this piezo beam shown in figure 3.6 was measured. Using a Data Acquisition box the voltage of generated by the piezo can be measured. The test setup is shown in 5.2. The piezo is manually plucked and the response of the system is measured over a 200k Ω resistor.

The resulting measurement is shown in figure 5.3a. The DAQ device used clips at ± 10 V. It can be noticed in the graph the voltage initially behaves erratic, but after a few seconds it starts resonating in its eigenfrequency. From this a fast fourier transform (FFT) can be done to examine the behaviour of the piezo beam. Because of the erratic behaviour initially, to get a better result this should be left out of the FFT. The range over

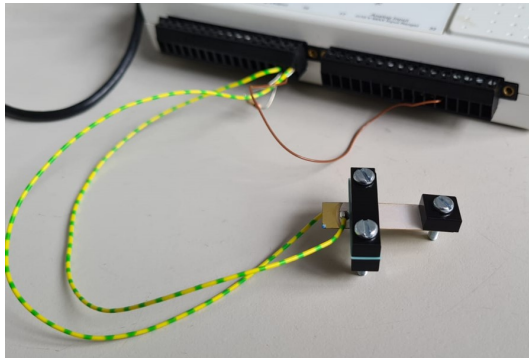
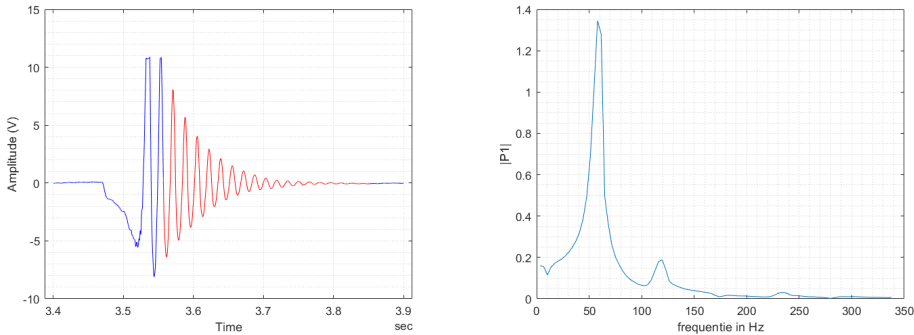


Figure 5.2: The test setup for manually plucking the piezo and measuring the voltage generated using a DAQ device. The voltage is measured over a 200kΩ resistor

which the FFT is applied is shown in red. This area is chosen so no clipping occurs within the data and the beam is freely vibrating. The generated single sided spectrum can be seen in 5.3b.



(a) The measured amplitude over a 100kΩ resistor. The part in red shows the part of the signal used for the FFT (b) The resulting FFT. The peak shows around 60Hz.

Figure 5.3: The measurement results of the plucking of the piezo beam. In (a) the time data of the measurements is shown. In (b) the FFT of the system is shown.

5.2.2. STIFFNESS ESTIMATE

The stiffness of the laser cut piezo was experimentally found. In 5.4 the setup is shown. A PM-505 motion stage is used to apply the desired displacements. A FUTEK LRM200 force sensor is used together with a national instruments DAQ device.

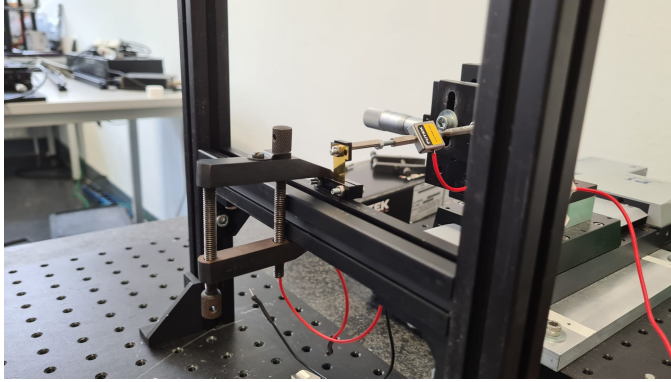


Figure 5.4: Measurement of the stiffness of the piezo beam. A motion stage is used to push a force sensor against the piezo beam. A DAQ device registers this force.

5

The generated graph can be seen in figure 5.5. The graph consist of the measurement made on the piezo and a straight line which represents the estimate stiffness. The measurements shows 2 lines to represent both directions. The straight line is a constant stiffness of 480 N/m which was found by manually adjusting the slope of the line until a line was found which represents the measured force deflection graph best.

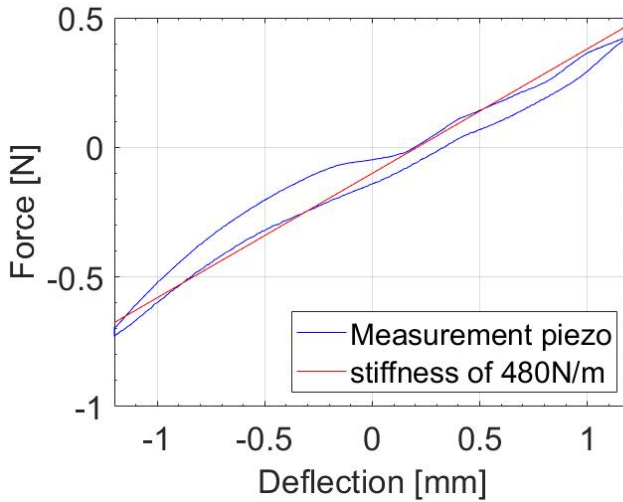


Figure 5.5: The generated force deflection graph of the T-shaped piezo buzzer. The red line drawn shows a straight line which represents a constant stiffness of 480 N/m

The piezo beam with tip mass can be represented as a single mass-spring-damper system. This means the eigenfrequency can be estimated with the formula shown in equation 5.1

$$f_n = \frac{1}{2\pi} \sqrt{\frac{k}{m}} \quad (5.1)$$

In this equation the k is the stiffness of the piezo beam, in this case 480N/m is used. The m is the tip mass added, which is 4g. Entering these values gives $f_n = 55.1Hz$. This value lies very close to the measured eigenfrequency from the FFT.

5.2.3. DAMPING ESTIMATE

The damping of the T-shaped piezo beam is found experimentally. To find this the plucking measurement from 5.3a can be used. The logarithmic decay method is applied.

LOGARITHMIC DECAY METHOD

The logarithmic decay method is used to find the damping of a system. For this a free vibration measurement is needed to analyse. A freely oscillating part of the signal is taken and the peaks are identified, as shown in figure 5.6.

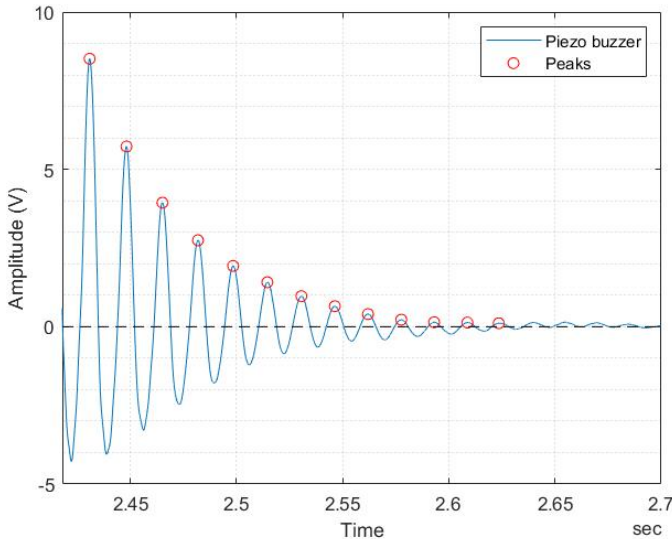


Figure 5.6: The measured voltage signal with peaks identified, used for determining the damping factor.

An initial peak is defined as t_0 and every following peak is named until the last peak t_n where n is dependent on the amount of peaks used. The logarithmic decrement δ needs to be determined with equation 5.2.

$$\delta = \frac{1}{n} \log \left(\frac{x(t_0)}{x(t_n)} \right) \quad (5.2)$$

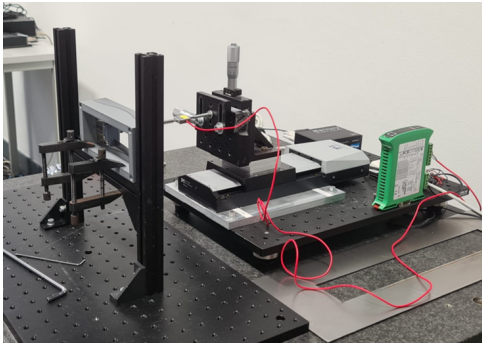
The $x(t_n)$ is the value of the peak at that certain time. From this logarithmic decrement value the damping coefficient ζ can be determined with equation 5.3

$$\zeta = \frac{\delta}{\sqrt{4\pi^2 + \delta^2}} \quad (5.3)$$

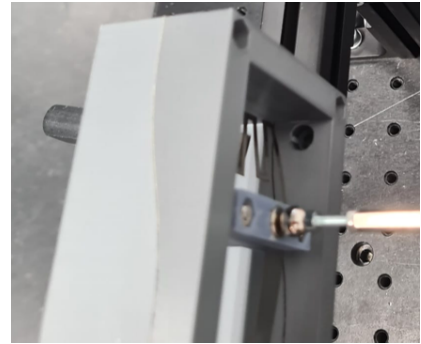
The damping coefficient for this wave is determined to be $\zeta = 0.0532$

5.3. VERIFICATION ANSYS MODEL

The FEM model made was experimentally validated. For this a FD-stage was used. This stages allows to apply a displacement and using a force sensor the FD-behaviour can be found. This stage is shown in figure 5.7a. The stage used is a PM-505 motion stage. The force sensor used is the FUTEK LRM200. Because of the bi stability of this design a magnet was also used for this measurement. This magnet ensures the system made contact in both directions of the movement, shown in figure 5.7b. The ball shape allows for the magnet to roll over the surface and thus apply a force normal to the mass block.



(a) The force deflection stage used. Consisting of a motion stage, a force sensor and a data acquisition unit.



(b) The ball magnet in contact with the design, o ensure contact with the system when snap through occurs.

Figure 5.7: The force deflection stage used shown in (a) and the contact with the bistable design shown in (b)

The simulated and measured force deflection behaviour is shown in 5.8. Both the measurement and simulation consist of 2 lines, showing the behaviour for movement in both directions. In the graph spikes can be noticed, which are not visible in the measurements. These spikes appear due to Ansys having inaccuracies when snap through behaviour appears.

The measurement shows the bi-stable behaviour of the system. In the stable points if the mass block is pushed away the forces push it back to the stable point. The stable points occur at $\pm 7.4\text{mm}$, which gives the distance between the stable points at 14.8mm from each other. The simulation is able to reasonably predict the behaviour of the folded flexure.

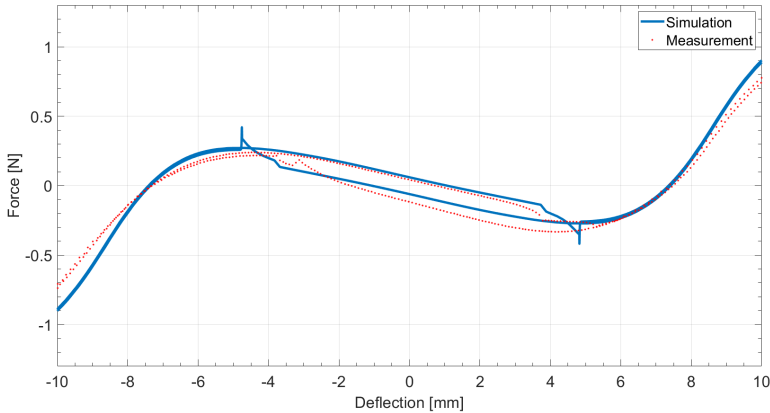


Figure 5.8: The force deflection of the bistable design graphed. In this the simulation is shown in blue and the measurements in red dots.

5.4. ACCELERATION SWEEP

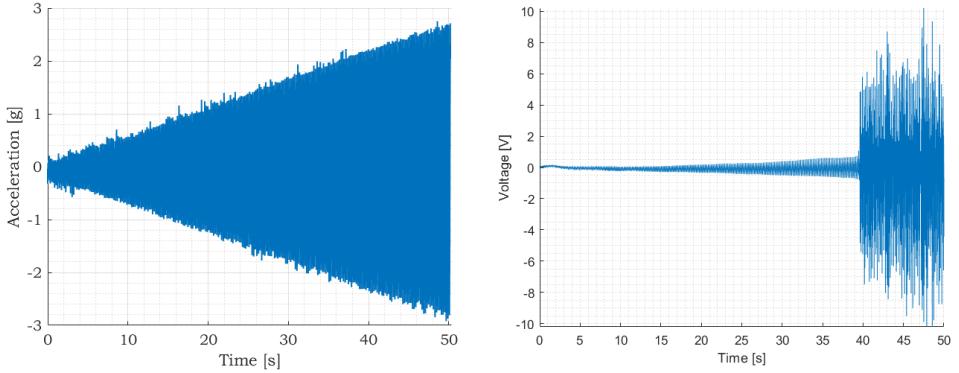
An experiment is performed to verify at which acceleration the BISup starts its snap through behaviour. For this a motion stage is used shown in figure 5.9. Shown here is a linear air bearing stage with a stroke of 500mm. This stage allows for experiments with low frequency signals.



Figure 5.9: The motion stage used for the acceleration sweep measurement. It is a linear air bearing stage with a 500mm stroke range. The high stroke allows for low frequency measurements.

The BISup design is measured when applying an acceleration sweep signal. This could give insight in the snap through behaviour of the design. The signal applied to the BISup is an acceleration sweep with a frequency of 5Hz and the accelerations range from 0g to 3g. Here g is the gravitational constant with a value of 9.81ms^{-2} . These value for the input signal were chosen to allow the design to snap through, while not the boundaries of the motion stage. The measurements are shown in figure 5.10. In figure 5.10a the

reference signal is measured to verify the input of the motion stage. In figure 5.10b the measurement of the voltage value of the piezo is shown.



(a) Measured signal of the acceleration sweep. This signal is measured on the motion stage with the use of an accelerometer.

(b) Measured voltage output of the piezo during the acceleration sweep.

Figure 5.10

In figure 5.10b some interesting behaviour can be noticed. At lower frequency's the system is generating a low voltage, due to the system not switching. Then at the 40 seconds mark the voltage increases a lot. This happens at an acceleration of about 2.2g. In figure 5.8 the force deflection behaviour was shown for the BISup. With Newton's second law, shown in equation 5.4, the acceleration at which snap through should occur can be calculated.

$$F = ma \quad (5.4)$$

The snap through force of the simulation is 0.27 Newtons. The mass attached to the frame is weighed to be 12 grams. Entering these values gives: $a = 22.5\text{ms}^{-2} = 2.3\text{g}$. This value lies very close to the value found using the acceleration sweep.

5.5. DYNAMIC MODEL

In chapter 3 the schematic model for the design was shown. The equations for this model were shown and are repeated below in equation 5.5

$$\begin{aligned} m_1 \ddot{x}_1 &= -k_1 x_1 - c_1 \dot{x}_1 + c_p (\dot{x}_p - \dot{x}_1) + k_p (x_p - x_1) \\ m_p \ddot{x}_p &= -c_p (\dot{x}_p - \dot{x}_1) - k_p (x_p - x_1) \end{aligned} \quad (5.5)$$

This model can be implemented in MATLAB to simulate the behaviour of the system. For this the unknown parameters need to be found. The equation shown in 5.5 is modified to create the equation shown in equation 5.6

$$\begin{aligned} m_1 \ddot{x}_1 &= -F_{k_{sys}} - F_{damp} - c_1 \dot{x}_1 + c_p (\dot{x}_p - \dot{x}_1) + k_p (x_p - x_1) \\ m_p \ddot{x}_p &= -c_p (\dot{x}_p - \dot{x}_1) - k_p (x_p - x_1) \end{aligned} \quad (5.6)$$

In this equation the $F_{k_{sys}}$ is used directly and can be found using the simulation made in ANSYS. This variable is dependent on not only x_1 but also the history of x_1 to determine from which path the force should come. The F_{damp} is an extra damping force when the system goes past the stable point. In this regime the system is extra damped which was not accounted for in the original equation.

5.5.1. SINGLE MASS SPRING DAMPER SYSTEM

To initially tune the design the system is simplified to a single mass-spring-damper system, shown in figure 5.11.

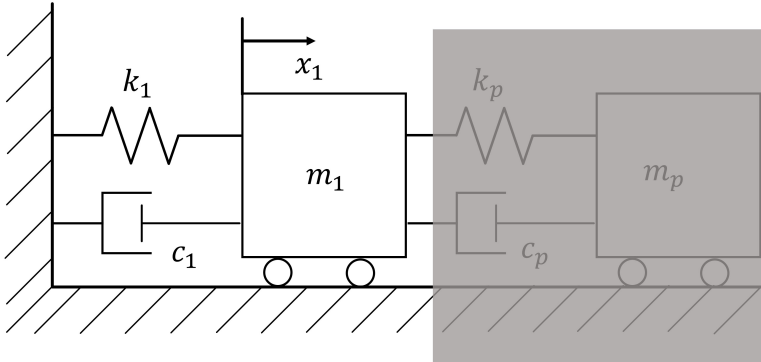


Figure 5.11: The model simplified to a single mass-spring-damper system.

The simplification to a single mass-spring-damper system results in a smaller equation of motion, shown in 5.7

$$m_1 \ddot{x}_1 = -F_{k_{sys}} - F_{damp} - c_1 \dot{x}_1 \quad (5.7)$$

In this equation the $F_{k_{sys}}$ can again be found using the ANSYS model. Using the equation shown in 5.7 the behaviour of the bi-stable system can be modelled dynamically. The F_{damp} is an extra damping which occurs when the system goes past its stable point, and is modelled by applying a bouncing coefficient when the system goes past a certain point

5.5.2. DYNAMIC MODEL SIMULATION

The single mass-spring-damper system discussed previously is simulated using the ODE45 solver in MATLAB. Equation 5.7 is implemented and a few variables are necessary. The $F_{k_{sys}}$ can be found using the ANSYS simulation results. A lookup table is made which interpolates between the data points made. A quick function gives $F_{k_{sys}}$ from the current x_1 and its history. One of the paths is chosen.

5.5.3. MODEL VERIFICATION

To verify the dynamic model the behaviour of the bi-stable flexure is measured and compared to the single-mass-spring-damper system. To measure how the system vibrates in

its stable point a laser sensor was used. The laser (a Keyence LK-H052) has a range of $\pm 10\text{mm}$. The laser was nulled in such a way the location was measured after switching and in the stable point. The measurement setup is shown in figure 5.12.

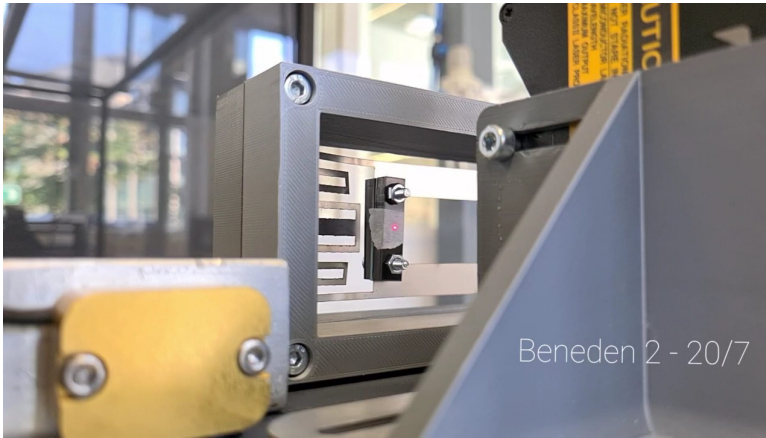


Figure 5.12: Measurement of the design. A Keyence laser sensor is used to measure the displacement of the mass block. The design is manually pushed to the switching point of the system, after which the design flips to the other stable position and vibrates.

5

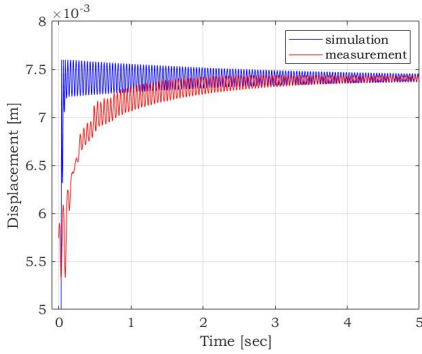
Two measurements made are shown in figure 5.13. One measurement shows the displacement switching towards the laser, the other shows the displacement switching away from the laser. The system is not fully symmetric, thus 2 different plots are shown. Also shown in this image is the single sided power spectrum of both measurements. This was made using a FFT and gives insight in the resonance frequency of the design.

In figure 5.13a the measurement shows some unexpected behaviour. While the simulation immediately oscillates about the stable point, the measurement seems to converge towards this stable point. This is unexpected behaviour and could mean the FD-graph cannot fully predict the behaviour of this system. This converging to the stable value could be due to a measurement error using this method or rotation are affecting the measured distance.

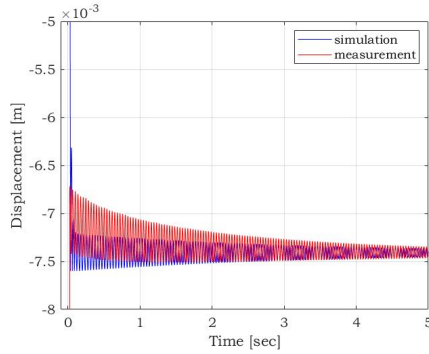
In figure 5.13b the results after switching away from the laser are shown. The measurement shows a line coming from below -8mm displacement. However, this line occurred when the mass block moved from in range of the laser. Again the system seems to converge to stable point in this measurement.

In figure 5.13c the single sided spectrum of the measurement signal from figure 5.13a is shown. This measurement shows the main frequency in which the flat flexure is oscillating. With this peak occurring at 23 Hz. The simulation oscillating frequency is found to be 26Hz.

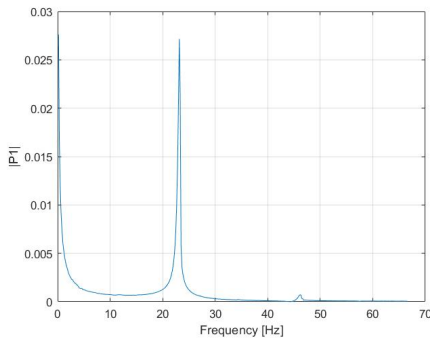
In figure 5.13d the single sided spectrum of the measurement signal from figure 5.13b is shown. This graph again gives the main frequency in which the flat flexure is oscillating. This frequency is found to be 27Hz. When analysing the simulation frequency it is again found to be at 26Hz. This shows the model can reasonably predict this behaviour for our system.



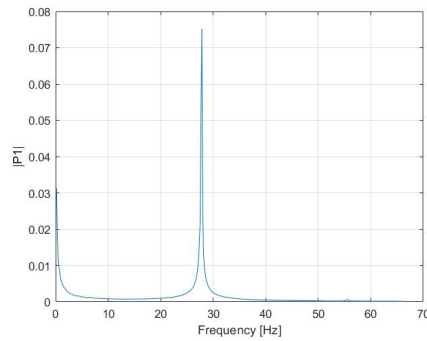
(a) Measurement after switching towards the laser side. The simulation of the system doing the same switching movement.



(b) Measurements after switching away from the laser



(c) Single sided power spectrum of the measurement towards the laser side. The peak is located at a frequency of 23 Hz.



(d) Single sided power spectrum of the measurement away from the laser side. The peak is located at a frequency of 27 Hz.

Figure 5.13: The plots (a) and (b) show the displacement of the system in both measurement and simulation. Plots (c) and (d) give the single sided power spectrum of the earlier mentioned plots respectively.

5.6. CONCLUSIONS

In this chapter a model of the energy harvester is presented. This model is based on a double mass-spring-damper system and can be used to predict the behaviour of the energy harvester. Each of the different properties necessary for the model is experimentally found. The force-deflection behaviour of the flat flexure is simulated and this simulation is verified using a measurement on the fabricated flat flexure.

An acceleration sweep is applied to the BISup design. From this a value for the snap through acceleration could be found and linked to the force deflection measurements.

The model is first simplified to a single mass-spring-damp system to verify if the behaviour of the flat flexure can be correctly predicted. The switching of the flat flexure from one stable point to the other is simulated and compared to a measurement performed with a laser. This test showed the model can reasonably predict the oscillating of the flat flexure. However, the measurement showed the system converges towards the

stable point and does not oscillate around the stable point. A focus could be to research why this difference between measurement and simulation occurs.

The next step would be testing the single mass-spring-damper system on more dynamic excitations and seeing if the model can still predict its behaviour. Finally the double mass-spring-damper system can be simulated to fully model the behaviour of the energy harvester design. If the full model is able to predict the behaviour of the design, then the flat flexure can easily be simulated to find an optimal design for its purpose.

6

CONCLUSION

This is a concluding chapter explaining the scientific and technical implications for society of the research findings in considerable detail.

6.1. OVERVIEW OF RESEARCH ACTIVITIES

This research started on September 1st 2020 and was concluded on May 17th 2022. An overview of the research activities performed are shown in figure 6.1. In this overview the flow of the project is shown and the key topics are shown in coloured blocks.

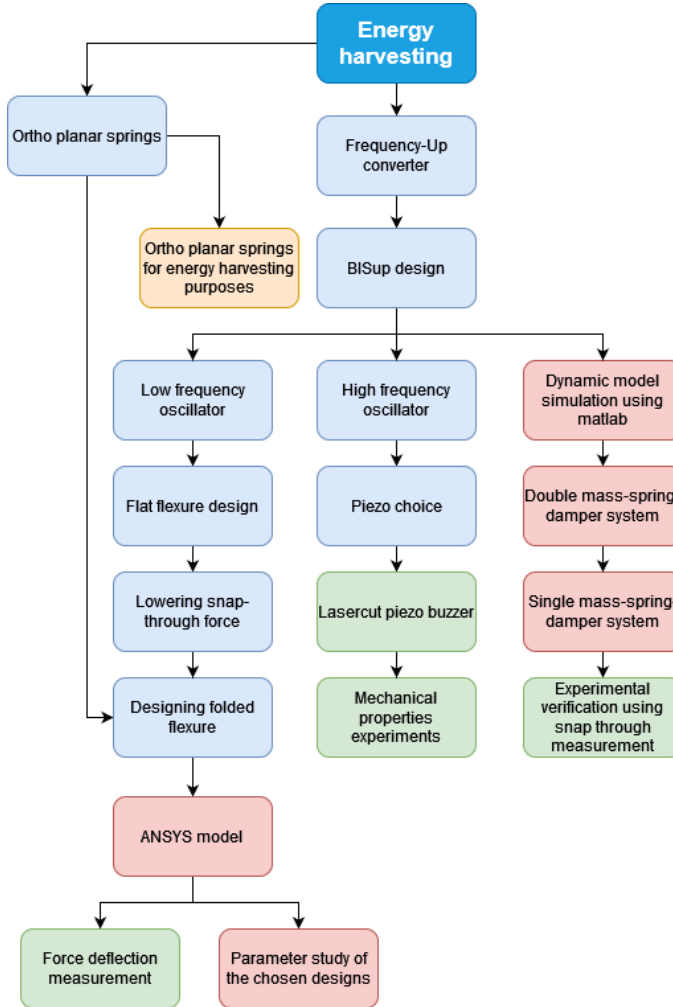


Figure 6.1: A figure showing an overview of the research activities performed. In blue the main flow of the project is shown. In red the modelling and simulations are shown. All experimental work is shown in red and finally the literature research is shown in yellow

6.2. SUCCESSES

A thesis consists of little projects, which together help make the big picture. Some parts worked out for the better and are described in this chapter.

6.2.1. BISUP DESIGN

The Bi-stable Impact-based Snap-through frequency-up converter (BISup) was designed and fabricated. Fabricating this energy harvester gave insight into the different factors required for an effective harvester. Fabricating such a design consists of multiple iterations to get the device as desired.

6.2.2. ANSYS MODEL

To gain more insight in the bi-stable system an ANSYS model was needed. Understanding and utilising this program was an important step to generating all the different force deflection graphs. This model was an important piece of this final research and performed good when compared to a physical measurement.

6.3. UNSUCCESSFUL EFFORTS

Performing research also consist out of attempting something and the outcome not behaving as expected. While these efforts did not always lead to the expected result, still information could be learned from these attempts.

6.3.1. BI-MORPH PIEZO

The Bi-Morph piezo initially used did not behave as expected. Due to its high stiffness, exciting the piezo in its eigenfrequency proved to be relatively difficult. Eventually it was decided to work with a piezo buzzer as this design could easily be laser-cut and thus the design was easily adjustable.

6.3.2. DOUBLE MASS-SPRING-DAMPER MODEL

A Double mass-spring-damper system was designed to represent the BISup. However, implementing the system seemed more difficult than expected. A lot of variables were dependent on earlier results which proved to be difficult to implement in the MATLAB model made.

6.4. RECOMMENDATIONS

First, the model made could be improved, to better predict the behaviour of the energy harvester. If this model is improved, an optimization study can be executed to find the ideal parameters for the desired use. The model could also be improved by more research into a piezo transducer. A piezo buzzer was used, but this buzzer had a lot of unknown properties, which needed to be determined. Using a piezo material which can easily be applied to a system could result in easier integration. An piezo material which can be attached to the steel used could result in a significantly flatter design.

Secondly, this research showed the use of ortho planar springs could increase the performance of energy harvesters. The next step would be implementing these ortho planar springs in an existing designs and seeing how this energy harvester would perform against other designs.

6.5. CONCLUSION

Vibration energy harvesting could be an interesting field for powering low power sensors or devices in hard to reach places. Energy harvesters can be used, but the design has to accommodate for the vibrations available. A frequency-up converter design can be used to accommodate for the difference between the available frequencies and the required frequencies for the transducer used.

Ortho planar springs is an interesting field to implement in the designs of frequency-up converters. Ortho planar springs are springs fabricated in one plane with its main direction of movement orthogonal to this plane. Using the ortho planar springs a bi-stable system can be affected, while still using the same design space. Big advantage of the use of ortho planar springs is the ease of fabrication and the ease of manipulation of stiffness. Dhote et al. [16] proposes the use of ortho planar spring design could be used to get a wide bandwidth of operation. However, the frequencies this design oscillates at is relatively high. The BISup design allows for operation at lower frequencies.

A Bi-stable Impact-based Snap-through frequency up converter (BISup) design was made. Earlier work [9] showed a device, using the same principles as the BISup, able to function at low frequency excitation. The BISup was used to gain knowledge on the behaviour of the bi-stable flat flexure. The bi-stable unit was investigated and multiple ortho planar spring designs were made to affect the snap through force needed. The simulations done in ANSYS showed the use of these designs did affect this. Using a ortho planar spring design could lower the force needed to snap through. This could lower the acceleration needed for snap through, thus improving the behaviour of this frequency up-converter. As can be seen in chapter 4, the horizontal design allows for the lowest snap-through force, and is probably best for using in this design. The reason for the lowered stiffness is due to this design allowing for the longer flexures, but it should be noted the designs with more legs did not lower the switching force significantly. However, for the horizontal design the lowered stiffness in its stable points could affect this design and further research is necessary.

A dynamic model was created and verified to estimate the performance of the BISup design. This model based on a double mass-spring-damper system. Simplifying this model to a single mass-spring-damper system allowed for insight in the flat flexure dynamic behaviour. This model is simulated using Matlab and experimentally verified using a snap-through measurement.

This thesis gained insight in the use of ortho planar spring design to manipulate a bi-stable system. This bi-stable system can be used to make a frequency up converter design. This design can be used to fabricate a energy harvesting device which can operate at relative low frequencies.

A

APPENDIX: VERTICAL DESIGN SIMULATION

A.1. VERTICAL DESIGN

The parameter study applied to the vertical design is shown here. The vertical design is shown again in figure [A.1](#).

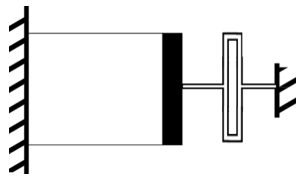


Figure A.1: Vertical design with a single fold

This design is simulated with an increased stabilization of $1e6$. By changing the width of the flexures the flexural rigidity is adjusted. The force deflection is simulated for the different widths and the results are shown in figure [A.2](#). The legend is flexural rigidity in Nm^2

A

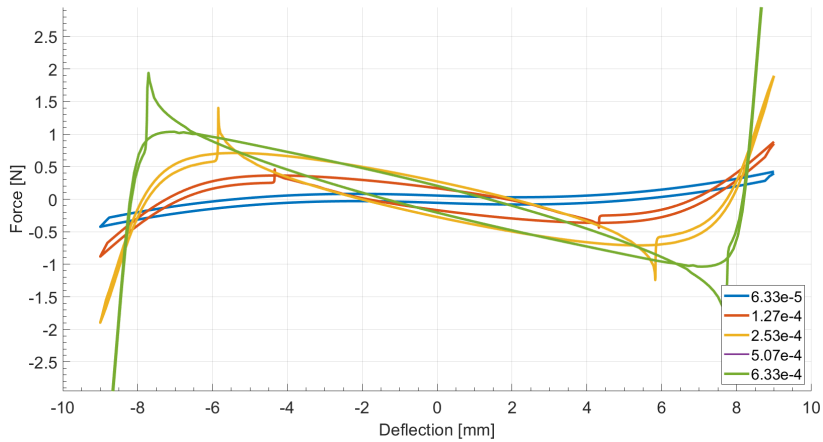


Figure A.2: Parameter study of the vertical single design. The legend shows the flexural rigidity of the folded flexure in Nm^2

The results show us expected behaviour. Increasing the flexural rigidity increases the stiffness of the design and the required force for snap through. The purple line seems to be missing. This is due to the solver not being able to compute the force deflection for this value. Also a lot of hysteresis can be noticed, which is due to the extra stabilization required for solving the parameter study. The vertical single designs seems to behave a little like the straight design.

B

APPENDIX: SNAP THROUGH VOLTAGE MEASUREMENT

B.1. SNAP-THROUGH EXPERIMENT BI-MORPH PIEZO

The BISup design with the bi-morph piezo is measured. The design is manually pushed until snap through occurs. The voltage output of the bi-morph piezo is measured using a National instruments DAQ device. The results are shown in figure B.1.

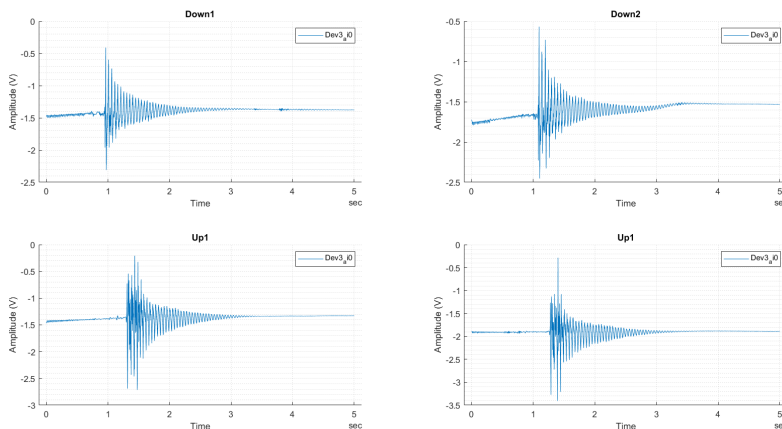


Figure B.1: The output of the snap through measurement. This measurement was done in different directions to check if it impacts the result.

From these measurement a quick FFT can be made to check the main frequencies present in this signal. The resulting figure is shown in figure B.2.

From these single sided spectra the main frequency of the flat flexure can be found. The main frequency occurring in the system is around 21Hz. Also something to note

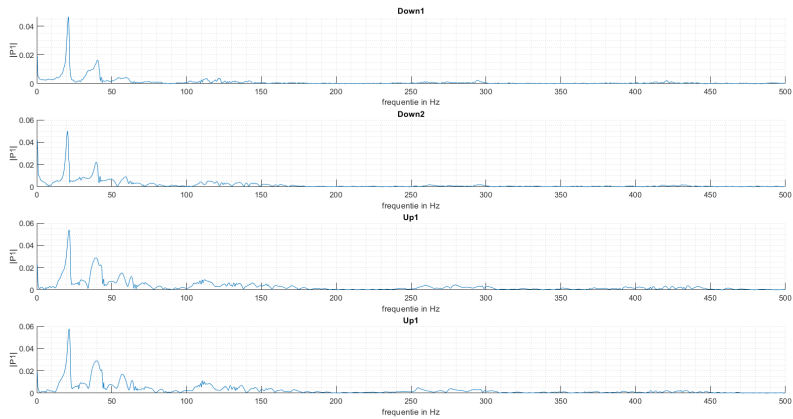


Figure B.2: The single sided spectrum generated from the fast fourier transform applied. The main peak is around 21Hz.

is almost no peak at around 300 Hz. It was found this was the eigenfrequency of bi-morph piezo. The snap through did not bring the bi-morph piezo beam in resonance. Considering this another piezo was designed with a lower eigenfrequency.

B.2. SNAP-THROUGH EXPERIMENT PIEZO BUZZER

A laser cut piezo buzzer was then used, with a lower resonance frequency. This lower frequency was found in section 5.2.1 to be around 60Hz. A snap through measurement was performed, similar to the measurement done to the bi-morph piezo setup. The resulting figure is shown in figure B.3.

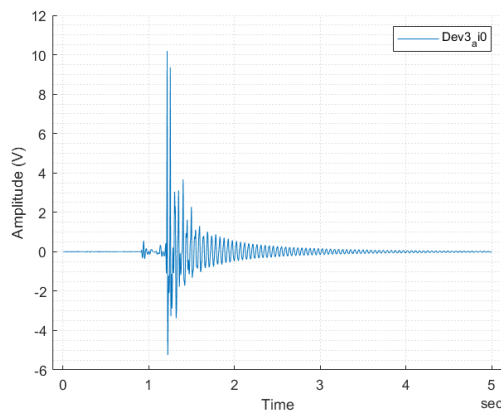


Figure B.3: Measured output of the piezo buzzer snap through test.

For this measurement a FFT is performed again. The signal is taken when the system is freely resonating from around 2 seconds. The resulting single sided spectrum is shown in figure B.4

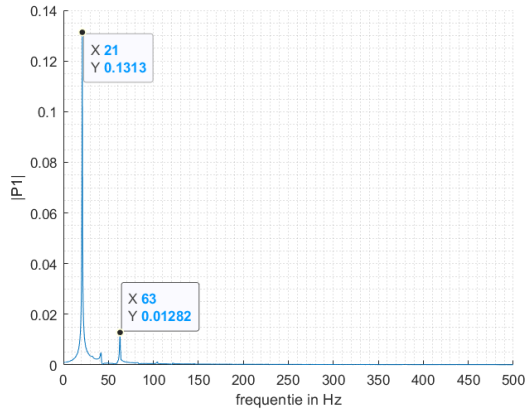


Figure B.4: The single sided spectrum generated from the fft on the signal shown. Peaks occur at 21Hz and 60Hz.

This shows again the frequency of 21 Hz is present in the system, due to flat flexure resonating. Another frequency present is at 63 Hz and can be explained due to the piezo buzzer resonating. This showed the piezo buzzer does resonate when snap through occurs.

C

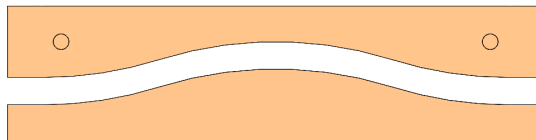
APPENDIX: PRELOAD DISTANCE

C.1. CURVED FRAMES

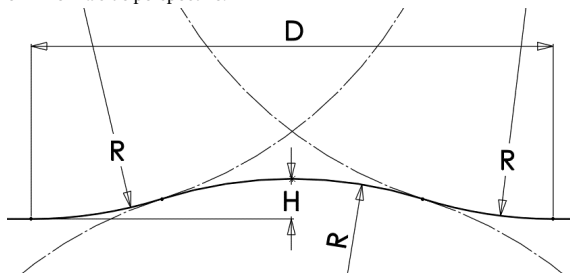
The curved frames are shown in figure C.1a. Schematically they are shown in figure C.1b. The curved frames consist of 3 arcs of equal radius tangent to each other. Equation C.1 calculates the distance preloaded (dL) [35].

$$dL = L - 2L_s - D = L - 2L_s - 4R \sin\left(\frac{L - L_s}{4R}\right) \quad (\text{C.1})$$

In this equation L is the initial length. L_s is the length of the straight part before the curvature starts. R is the radius of the 3 arcs and D is the shortened distance.



(a) The curved frames shown from a side perspective.



(b) The bottom curved frame schematically shown. The frame consists of 3 arcs tangent to each other.

Figure C.1

BIBLIOGRAPHY

REFERENCES

- [1] A. Dewan, S. U. Ay, M. N. Karim, and H. Beyenal, "Alternative power sources for remote sensors: A review," 2014.
- [2] M. Kindermann, B. Schwaab, M. Berg, and G. Fröhlig, "Longevity of dual chamber pacemakers: Device and patient related determinants," *PACE - Pacing and Clinical Electrophysiology*, vol. 24, no. 5, pp. 810–815, 2001.
- [3] S. Roundy, P. K. Wright, and J. Rabaey, "A study of low level vibrations as a power source for wireless sensor nodes," *Computer Communications*, vol. 26, pp. 1131–1144, jul 2003.
- [4] R. Riemer and A. Shapiro, "Biomechanical energy harvesting from human motion: Theory, state of the art, design guidelines, and future directions," *Journal of Neuro-Engineering and Rehabilitation*, vol. 8, p. 22, apr 2011.
- [5] G.-W. Kim and J. Kim, "Related content Compliant bistable mechanism for low frequency vibration energy harvester inspired by auditory hair bundle structures," 2012.
- [6] P. L. Green, E. Papatheou, and N. D. Sims, "Energy harvesting from human motion and bridge vibrations: An evaluation of current nonlinear energy harvesting solutions," *Article Journal of Intelligent Material Systems and Structures*, vol. 24, no. 12, pp. 1494–1505, 2013.
- [7] T. W. Blad and N. Tolou, "On the efficiency of energy harvesters: A classification of dynamics in miniaturized generators under low-frequency excitation," *Original Article Journal of Intelligent Material Systems and Structures*, vol. 30, no. 16, pp. 2436–2446, 2019.
- [8] M. Pozzi and M. Zhu, "Plucked piezoelectric bimorphs for knee-joint energy harvesting: Modelling and experimental validation," *Smart Materials and Structures*, vol. 20, p. 055007, may 2011.
- [9] S. M. Jung and K. S. Yun, "Energy-harvesting device with mechanical frequency-up conversion mechanism for increased power efficiency and wideband operation," *Applied Physics Letters*, vol. 96, no. 11, 2010.
- [10] J. J. Parise, L. L. Howell, and S. P. Magleby, "Ortho-planar linear-motion springs," *Mechanism and Machine Theory*, vol. 36, pp. 1281–1299, nov 2001.

- [11] O. Smal, B. Dehez, B. Raucent, M. De Volder, J. Peirs, D. Reynaerts, F. Ceyskens, J. Coosemans, and R. Puers, "Modelling and characterisation of an ortho-planar micro-valve," *IFIP International Federation for Information Processing*, vol. 198, pp. 315–326, 2006.
- [12] O. Smal, B. Dehez, B. Raucent, M. De Volder, J. Peirs, D. Reynaerts, F. Ceyskens, J. Coosemans, and R. Puers, "Modelling, characterization and testing of an ortho-planar micro-valve," vol. 4, pp. 131–143, 2008.
- [13] N.-T. Nguyen, T.-Q. Truong, K.-K. Wong, S.-S. Ho, C. Lee, and N. Low, "Micro check-valves for integration into polymeric microfluidic devices," tech. rep.
- [14] R. Graipaspong and T. Chanthasopeephan, "The Design of Ortho-Planar Spring for a Normally-Closed Gate Valve," in *2018 International Conference on Reconfigurable Mechanisms and Robots, ReMAR 2018 - Proceedings*, Institute of Electrical and Electronics Engineers Inc., aug 2018.
- [15] C. H. Cheng and Y. P. Tseng, "Characteristic studies of the piezoelectrically actuated micropump with check valve," in *Microsystem Technologies*, vol. 19, pp. 1707–1715, Springer, nov 2013.
- [16] S. Dhote, J. Zu, and Y. Zhu, "A nonlinear multi-mode wideband piezoelectric vibration-based energy harvester using compliant orthoplanar spring," *Applied Physics Letters*, vol. 106, apr 2015.
- [17] A. Cammarano, S. G. Burrow, and D. A. W. Barton, "Modelling and experimental characterization of an energy harvester with bi-stable compliance characteristics," *Proceedings of the Institution of Mechanical Engineers, Part I: Journal of Systems and Control Engineering*, vol. 225, pp. 475–484, jun 2011.
- [18] S. M. Soliman, M. Abdel-Rahman, E. F. El-Saadany, and R. R. Mansour, "A wideband vibration-based energy harvester," *JOURNAL OF MICROMECHANICS AND MICRO-ENGINEERING J. Micromech. Microeng*, vol. 18, p. 11, nov 2008.
- [19] M. Safaei, H. A. Sodano, and S. R. Anton, "A review of energy harvesting using piezoelectric materials: State-of-the-art a decade later (2008-2018)," *Smart Materials and Structures*, vol. 28, p. 113001, oct 2019.
- [20] H. Elahi, M. Id, and Eugeni, and P. Gaudenzi, "A Review on Mechanisms for Piezoelectric-Based Energy Harvesters," *mdpi.com*, 2018.
- [21] F. Qian, T. B. Xu, and L. Zuo, "Piezoelectric energy harvesting from human walking using a two-stage amplification mechanism," *Energy*, vol. 189, p. 116140, dec 2019.
- [22] F. Qian, M. R. Hajj, and L. Zuo, "Bio-inspired bi-stable piezoelectric harvester for broadband vibration energy harvesting," *Energy Conversion and Management*, vol. 222, p. 113174, oct 2020.
- [23] J. West, "Scholar Commons Orthoplanar Spring Based Compliant Force/ Torque Sensor for Robot Force Control," tech. rep., 2017.

- [24] C. Qiu, P. Qi, H. Liu, K. Althoefer, and J. S. Dai, "Six-Dimensional Compliance Analysis and Validation of Orthoplanar Springs," *Journal of Mechanical Design, Transactions of the ASME*, vol. 138, apr 2016.
- [25] F. Hu, Z. Li, Y. Qian, al, I. Khan, R. Ben Mrad -, H. Ren, F. Tao, W. Wang, L. Schmitt, W. Wang, and J. Yao, "An electrostatic mems spring actuator with large stroke and out-of-plane actuation," *IOP PUBLISHING JOURNAL OF MICROMECHANICS AND MICROENGINEERING J. Micromech. Microeng*, vol. 21, pp. 115029–115036, nov 2011.
- [26] G. H. Teichert and B. D. Jensen, "Design and fabrication of a fully-compliant mechanism for control of cellular injection arrays," *Production Engineering*, vol. 7, pp. 561–568, sep 2013.
- [27] K. Wang, X. Shao, X. Dai, Z. Yang, G. Ding, and X. Zhao, "A Planar Architecture with Dual-Nonlinearity for Bandwidth Extension of a Multi-Modal Energy Harvester," *ieeexplore.ieee.org*, 2020.
- [28] Y. Tian, C. Zhou, F. Wang, K. Lu, and D. Zhang, "A novel compliant mechanism based system to calibrate spring constant of AFM cantilevers," *Sensors and Actuators, A: Physical*, vol. 309, p. 112027, jul 2020.
- [29] G. Hao, F. Dai, X. He, and . Y. Liu, "Design and analytical analysis of a large-range tri-symmetrical 2R1T compliant mechanism," *Microsystem Technologies*, vol. 23, pp. 4359–4366, 2017.
- [30] J. O. Jacobsen, B. G. Winder, L. L. Howell, and S. P. Magleby, "Lamina emergent mechanisms and their basic elements," *Journal of Mechanisms and Robotics*, vol. 2, pp. 1–9, feb 2010.
- [31] B. Scholarsarchive and H. Greenberg, "The Application of Origami to the Design of Lamina Emergent Mechanisms (LEMs) with Extensions to Collapsible, Compliant and Flat-Folding Mechanisms BYU ScholarsArchive Citation," tech. rep., 2012.
- [32] B. Scholarsarchive and J. O. Jacobsen, "Fundamental Components for Lamina Emergent Mechanisms BYU ScholarsArchive Citation," tech. rep.
- [33] K. Tao, S. W. Lye, J. Miao, and X. Hu, "Design and implementation of an out-of-plane electrostatic vibration energy harvester with dual-charged electret plates," 2015.
- [34] M. Deterre, "Toward an energy harvester for leadless pacemakers," 2013.
- [35] M. Mariello, T. W. Blad, V. M. Mastronardi, F. Madaro, F. Guido, U. Stauer, N. Tolou, and M. De Vittorio, "Flexible piezoelectric AlN transducers buckled through package-induced preloading for mechanical energy harvesting," *Nano Energy*, vol. 85, p. 105986, jul 2021.